13

Spatial distribution of Room Acoustics Parameters

The distribution acoustical quality inside concert spaces is not uniform (Akama et al. 2010, de Vries et al. 2001, Pelorson et al. 1992, Fujii et al. 2004). Source to receiver distances, as well as local conditions such as vicinity of sidewalls, balcony overhangs and balcony fronts make for substantial differences between listening positions. These differences can be measured by using the standard ISO 3382-1 room acoustic parameters. These measurements show that the differences between these listening positions can very well go beyond the JNDs (Barron 2005, Akama et al. 2010).

A clear objective of good acoustic design is to provide optimal acoustics to all listening positions inside a room. In this chapter we will look at the distribution of parameters in concert spaces and how room shape influences this distribution.

13.1 Past studies on distribution

Several studies have been made as to the variability in room acoustical parameters in different positions in concert spaces, in other words on their spatial distribution (Akama et al. 2010, de Vries et al. 2001, Pelorson et al. 1992, Fujii et al. 2004). In these studies distribution maps and histograms of different acoustical parameters are plotted in order to study their distribution. Although the object of the study is not a statistical fact, but a physical phenomenon at different points in the space, statistical methods such as histograms can be employed to best understand this distribution.

Akama et al. studied the spatial distribution for three different concert halls of varying shape, volume, and seating capacity. They measured the impulse response in almost every seating position in these rooms, and plotted both distribution maps and histograms of the distribution of several monaural parameters at mid frequencies. They calculated the width of the distribution for 90% of the values and found that this width is several times bigger that the JND, especially for EDT and C_{80} where it could reach more that 5 times the JND, less so for RT where it could reach less than 3 times the JND (Akama et al. 2010).

Akama et al. also performed normality tests on the histograms for RT, EDT and C_{80} values in these three rooms. Normality tests are meant to study the distribution in a histogram and determine wether or not the distribution can be considered normal. They found that many of the distributions, especially those involving C_{80} at mid frequencies, could not be said to have normal distributions.

Fujii et al. measured the impulse responses in many listening positions in two Japanese concert halls with similar shape but with different volume, seating capacity and surface types in their sidewalls (one more irregular than the other) (Fujii et al. 2004). They plotted distribution maps for the Sound Pressure Level (SPL), subsequent reverberation time (T_{sub}), Initial Time Delay Gap (Δt_1) and $IACC$. They confirmed that distributions of these parameters are wider their respective JNDs. They also concluded that the scattered reflections of the sidewalls of one of the rooms had an influence on the distribution, particularly by decreasing SPL and increasing Δt_1 values near the walls.

13.2 Measurements of Distribution

The ISO 3382-1 standard (ISO 3382-1:2009 International Standards Organization, 2009) parameters all measure values for single points in the room. So in order to quantify their distribution inside the room we need to resort to statistical or mathematical methods. This section discusses several methods for the study and quantification of this distribution. Additionally we look into the distribution of optimal values inside the room, rooms should not only be acoustically as uniform as possible, they should uniformly distribute optimal acoustics.

13.2.1 Average values

It is very common for acousticians to display room measurements in terms of whole room averages. They convey a general description of the room in a single, easy to understand value. However, mean values can be misleading because they can be the result of very different values. This might not be the case for reverberation times, but many other acoustical parameters such as Clarity and Sound Strength can vary greatly inside a single room (Barron 2005, 2013). This also means that two very different halls can share the same mean values. Barron makes the example of two british halls, one with favorable subjective impressions, and the other very much unliked by audiences, and points out that this could not be predicted by their average objective values. This means that their average values are quite similar despite their very different subjective impression(Barron 2005).

13.2.2 Standard deviation

The ISO 3382-1 standard (ISO 3382-1:2009 International Standards Organization, 2009) cites the Standard deviation (σ) as a way to describe spatial variance. The standard deviation is good way to present measurements in a room. For example, the mean value of C_{80} for all listening positions, accompanied by the standard deviation of those values from the mean, paints us a much clearer picture of how the clarity parameter is distributed inside this room.

It is worth noting that standard deviations have very little meaning in non-normal distributions. When we have asymmetrical distributions in terms of their mean value, the standard deviation can be misleading, and should not be taken into consideration. As we have seen above, not all distributions of acoustical parameters inside concert spaces are normal distributions. Hence the standard deviation is not a perfect indicator of distribution.

When we study how *optimal* values of acoustic parameters are spatially distributed inside the room (uniformly or not), the standard deviation is not a viable option. If we consider two rooms with the same average C_{80} but with different standard deviations, we can be sure that the room with the lowest standard deviation is the more uniform room. But if we want to figure out which room has the largest distribution of optimal C_{80} values, and the optimal C_{80} is not equal to the two rooms average C_{80} values, then the standard deviation is not going to help us. It could be the case that the room with the highest standard deviation has more listening positions with

optimal C_{80}.

Comparisons between rooms are quite useful in the design of a new room, especially if one considers the use of optimization or automated search algorithms. Uniformity for uniformity's sake is not enough to design a room. We need the evenly distribute an optimal value (typically a value related to subjective preference). The use of optimal values to determine a room's form presumes an agreement among the designers about these optimal values. Currently acousticians do not agree upon definite optimal values for most of the performance parameters contained in ISO 3382-1, and more importantly many lack criteria for preferred values (Bradley 2011). There is also disagreement on the correct parameters to use. However, since all current parameters describe the acoustical quality in a single point in the room, they all have a need for uniformity measures. They all also need optimal values relating to subjective preferences, so in order to design a room, an agreement among the people involved has to be reached.

13.2.3 Percentage of satisfied receivers

Barron (Barron 2005) proposed the use of the percentage of "satisfied" receivers as another possible number to describe the acoustic quality of a whole room. Receivers will be considered satisfied in a different way for each performance parameter in question. Generally speaking a receiver will be considered satisfied when it obtains a parameter value within a pre-selected optimal range. For example, if we select an optimal range of EDT from 1.8 to 2.2 seconds, then we will consider satisfied all of the receiver positions in which we can measure an EDT within that range. Some acoustic parameters are frequently studied in relation to the source-receiver distance. In this case the determination of a satisfied receiver can be made by means of a function that considers the source-receiver distance. For example, Barron proposes a minimum acceptable sound strength G value that is in relation to the source-receiver distance (Barron 2005). That value is determined by equation 12.6. So in this case we would consider satisfied receivers who obtain a G value equal of higher than G_{min}. In order for the percentage of satisfied receivers to work properly, a high number of measurements are required. This costly and labour intensive, but this can be expected on any measure of spatial distribution.

The percentage of satisfied receivers seems to be a good way of comparing rooms in terms of the spatial distribution of sound quality, the room with the highest percentage should be considered the best room. Since it is a percentage, it also has the advantage of communicating quite well the

degree in which the room is uniform or dis-uniform. The percentage of satisfied receivers however does not consider the degree in which the dissatisfied receivers are dissatisfied. Since this percentage looks only into the number of receivers that lie inside an optimal range, it does not measure the difference between the measured data and the optimal values, we do not get an idea of how far the unsatisfied are from being satisfied.

Figures 13.1 and 13.2shows an analysis of the unsatisfied receivers for a series of different shoebox rooms (A,B,C and D) with various room length to width ratios and heights. The analysis consists in the incremental widening of the optimal range from which the percentage of satisfied receivers is calculated. In the x axis we see how this range increases in size, and in the y axis we see the percentage of satisfied receivers corresponding to each range. By plotting the percentage as it increases with the wider ranges we get an clear picture of how close or how far receivers were from the original range. In other words, the faster the rate of increment of the percentage, the less unsatisfied the unsatisfied receivers are.

The first issue we can discuss about this graphs is the fact that the rate of increment of each room. We can see that the rates are always not constant, we see the percentage increase in curves with varying slope angles. If we look at the curves for EDT we can see that rooms C and D have higher initial numbers of satisfied receivers, but A and B have a very high rate when compared to C and D. So we can say that C and D have unsatisfied receivers that are more unsatisfied that those from A and B.

If we look at the case of C_{80} this behavior is perhaps even more evident. Rooms B and C have a higher initial percentage than room A, but room A has a much higher rate of increment, to the point that room A surpasses rooms B and C after a few range increments and reaches 100% first than them. We can generalize the results of this study by saying that a higher number of satisfied receivers does not guaranty that the unsatisfied receivers will be less unsatisfied. On the contrary, it could be argued that, in some cases, a high percentage of satisfied receivers is achieved at the expense of the unsatisfied ones. So if we have to compare rooms A and B for example, it's not so easy to say which is best, one that has a good number of satisfied receivers and the rest are completely unsatisfied (room B), or one that has a lower number of satisfied but the unsatisfied are not that unsatisfied (room A).

The unsatisfied analysis reveals that there is no straight forward relationship between the percentage of satisfied and the status of the unsatisfied. Hence, there is a need for a more precise tool in the study of the distribution of optimal values inside rooms. One that includes the unsatisfied receivers

in the equation.

13.2.4 Histograms Study

We have seen above that past studies on the distribution of acoustic parameters inside rooms employ the use of statistical tools such as histograms in their studies. We will begin this section by plotting the histograms for our test rooms A, B, C and D.

Figures figs. 13.3 to 13.7 show histograms of the distribution of RT, EDT, C_{80}, G and LF_{early} values at mid frequencies in rooms A, B, C and D. In the x axis they show the respective parameter values discretized in small sections and in the y axis they show the occurrence or frequency in which these values fall into. The charts also show the width of 90% of the distribution. We can also see in grey the optimal values for each parameter suggested for the symphony concert hall. The optimal values for each parameter and the source of the value (name and publication of author who suggested it) are presented in the following table:

Parameter	**Optimal Range**	**Reference**
RT	1.8 to 2.2 (s)	(Barron 2009*a*)
EDT	1.8 to 2.2 (s)	(Barron 2009*a*)
C_{80}	-2 to 2 (dB)	(Barron 2009*a*)
G	Barron's min G curve to ∞ (dB)	(Barron 2009*b*)
LF_{early}	0.1 to 0.35	(Barron 2009*a*)

RT histograms are shown in figure 13.3, they show that the distributions are usually very uniform, it is widely known that RT is mostly uniform throughout the room. With the exception of a few outliers in room B, most of the RT values lie within 2-3 JNDs from each other. In addition, the distributions seem to be symmetrical. Other parameters have less uniform and symmetrical distributions.

Figure 13.4 shows the EDT distributions, they show much wider distributions in terms of their JNDs, form 8 to 15 JNDs in width. We can also note that distributions are not very symmetrical.

Figure 13.5 shows the C_{80} distributions. Looking at these histograms we can explain the results of the unsatisfied analysis shown in figures 13.1 and 13.2. We can see why rooms B and C have a higher initial percentage of satisfied receivers. Many of their listeners lie inside the optimal range, but they are distributed in a wide area (12.5 and 9.4 JNDs respectively).

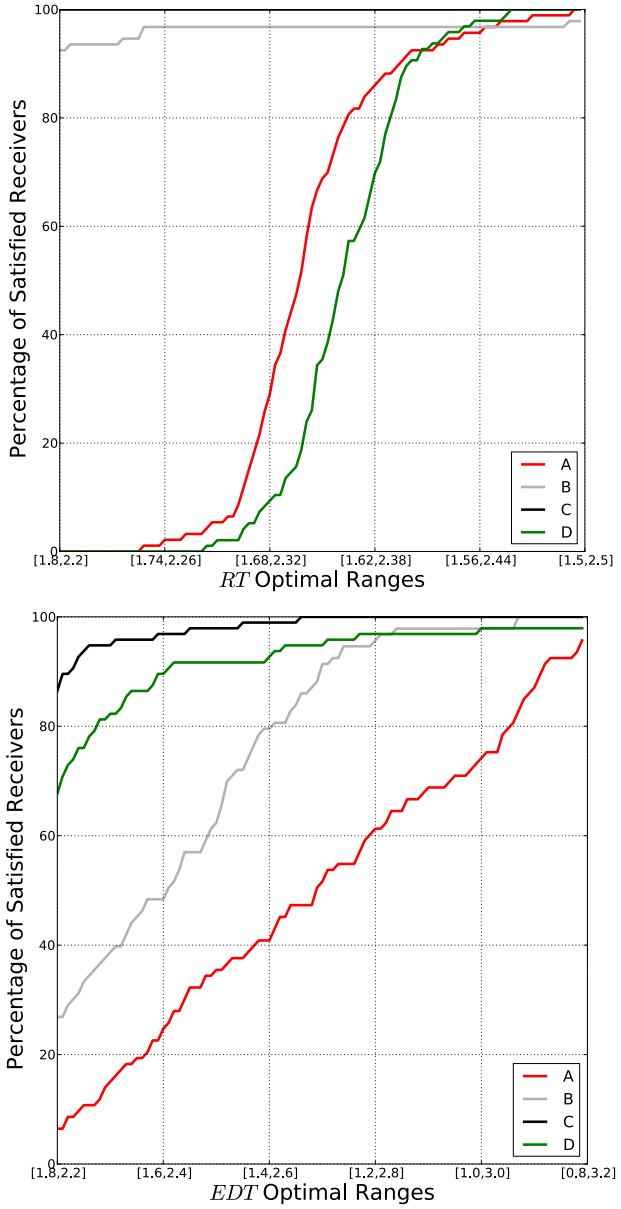

Figure 13.1: Unsatisfied analysis for RT, EDT, C_{80} and LF_{early} for rooms A and B.

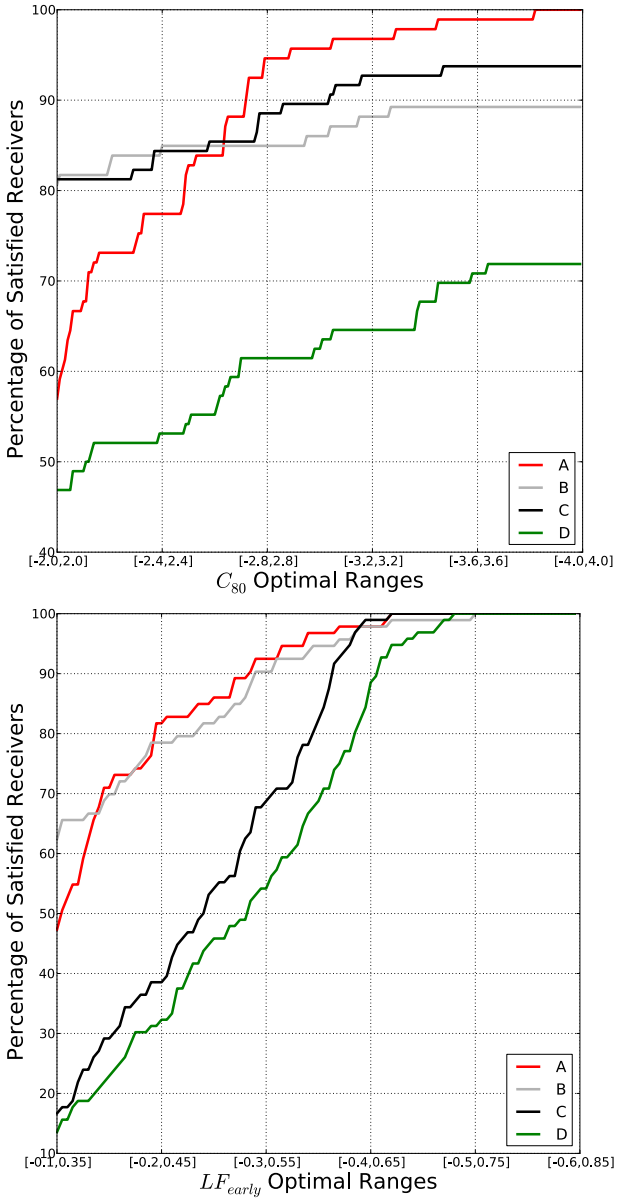

Figure 13.2: Unsatisfied analysis for RT, EDT, C_{80} and LF_{early} for rooms C and D.

Room A has a narrower distribution of 8.5 JNDs but it is not centered in the optimal range, however it is very close to the optimal values, hence its unsatisfied receivers are not as unsatisfied as those in rooms B and C. We can also see that these distributions are quite asymmetrical and far from a normal distributions.

13.2.5 Difference weighted sum

Based on Ando's theory of subjective preference (Ando 1983) Beranek devised an "objective method" that rated rooms according to the mean values of orthogonal objective attributes (Beranek 2004), in Beranek's case they were $IACC$, Δt_1, G_{mid}, EDT, BR and SDI. As it was outlined above, his rating is based on a weighted sum of 6 parameters. The rating method can be outlined with the following set of equations:

$$S = S_1 + S_2 + S_3 + S_4 + S_5 + S_6 \tag{13.1}$$

where S is the total subjective preference of an acoustical environment and $S_{i_{th}}$ is determined by:

$$S_i = a_i |x_i|^{3/2} \tag{13.2}$$

where:

$$\begin{array}{l} x_1 = 1 - IACC_{early} \\ x_2 = log(\Delta t_1 / \Delta t_{1,pref}) \\ x_3 = G_{mid} - G_{mid} \qquad \text{(dB)} \\ x_4 = log(EDT / EDT_{pref}) \\ x_5 = log(BR / BR_{pref}) \\ x_6 = log(SDI / SDI_{pref}) \end{array} \tag{13.3}$$

where $IACC$, Δt_1, G_{mid}, EDT, BR and SDI are the average values of those parameters, $IACC_{pref}$, $\Delta t_{1,pref}$, $G_{mid,pref}$, EDT_{pref}, BR_{pref} and SDI_{pref} are the optimal or preferred ranges of values of the same parameters, and where:

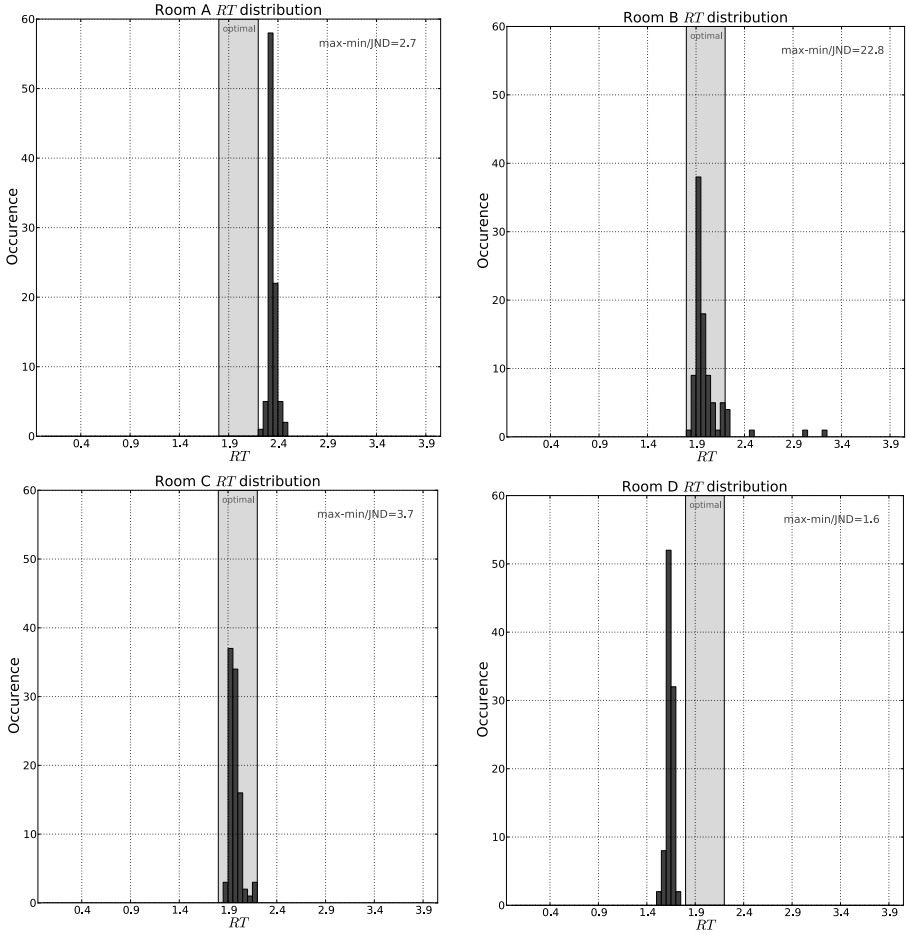

Figure 13.3: Histograms of the distribution of RT for rooms A, B, C and D.

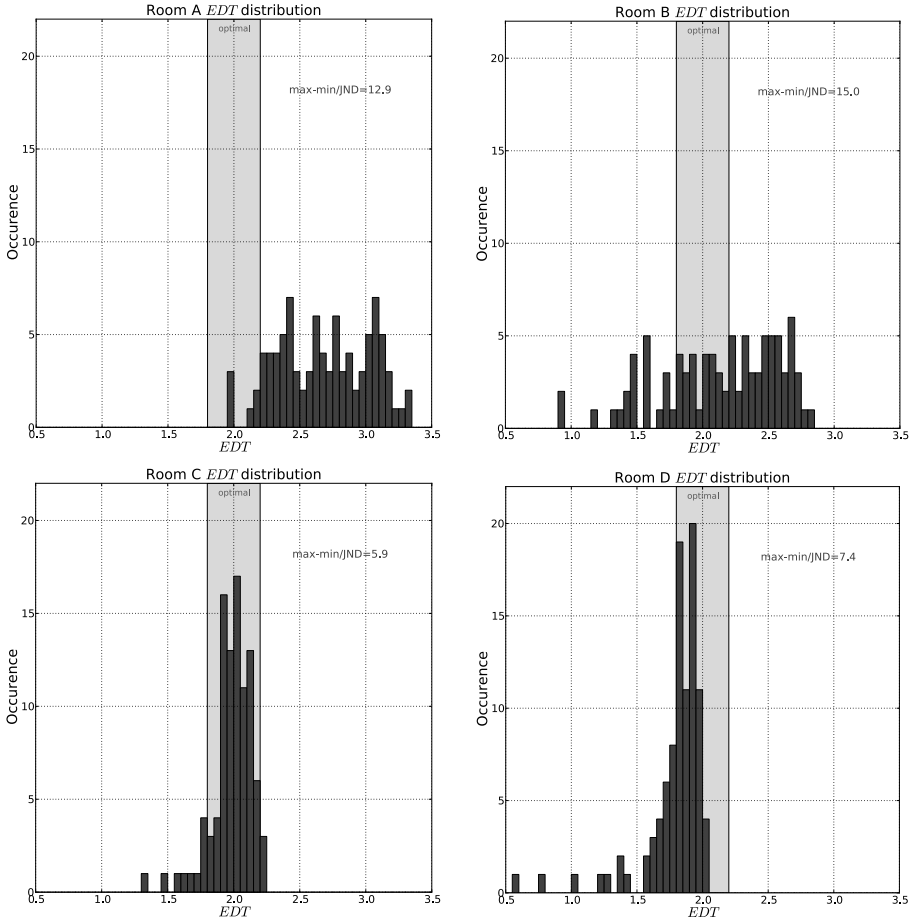

Figure 13.4: Histograms of the distribution of EDT for rooms A, B, C and D.

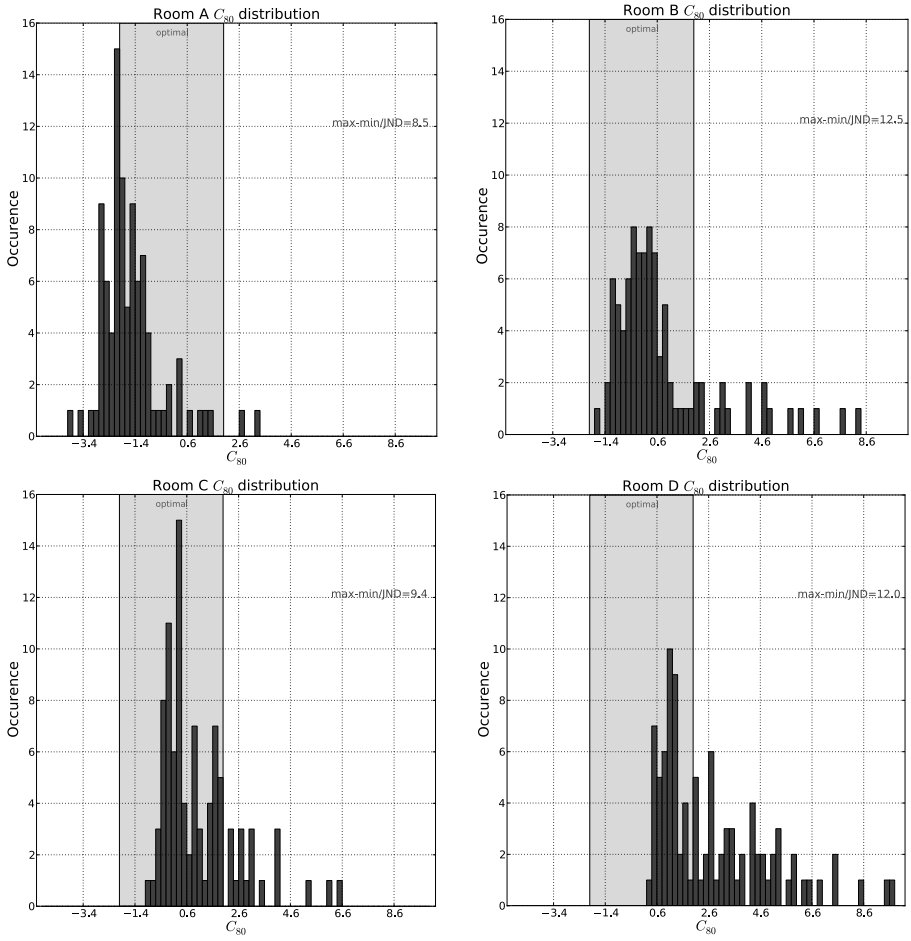

Figure 13.5: Histograms of the distribution of C_{80} for rooms A, B, C and D.

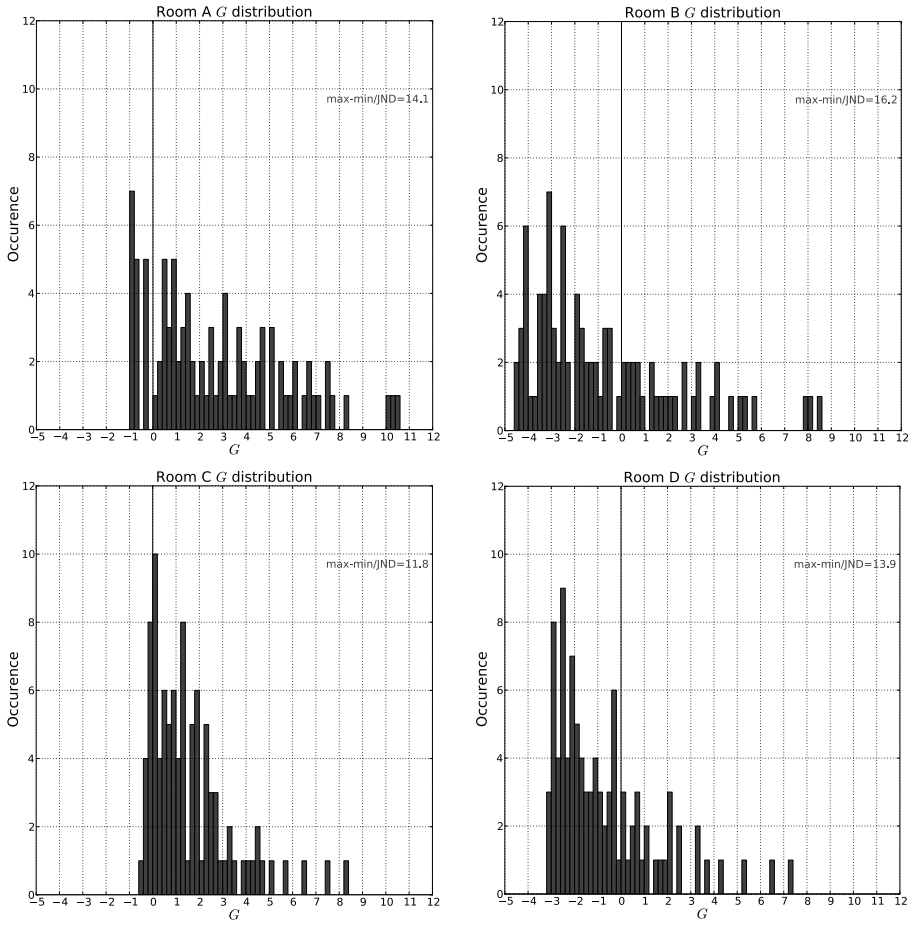

Figure 13.6: Histograms of the distribution of G for rooms A, B, C and D.

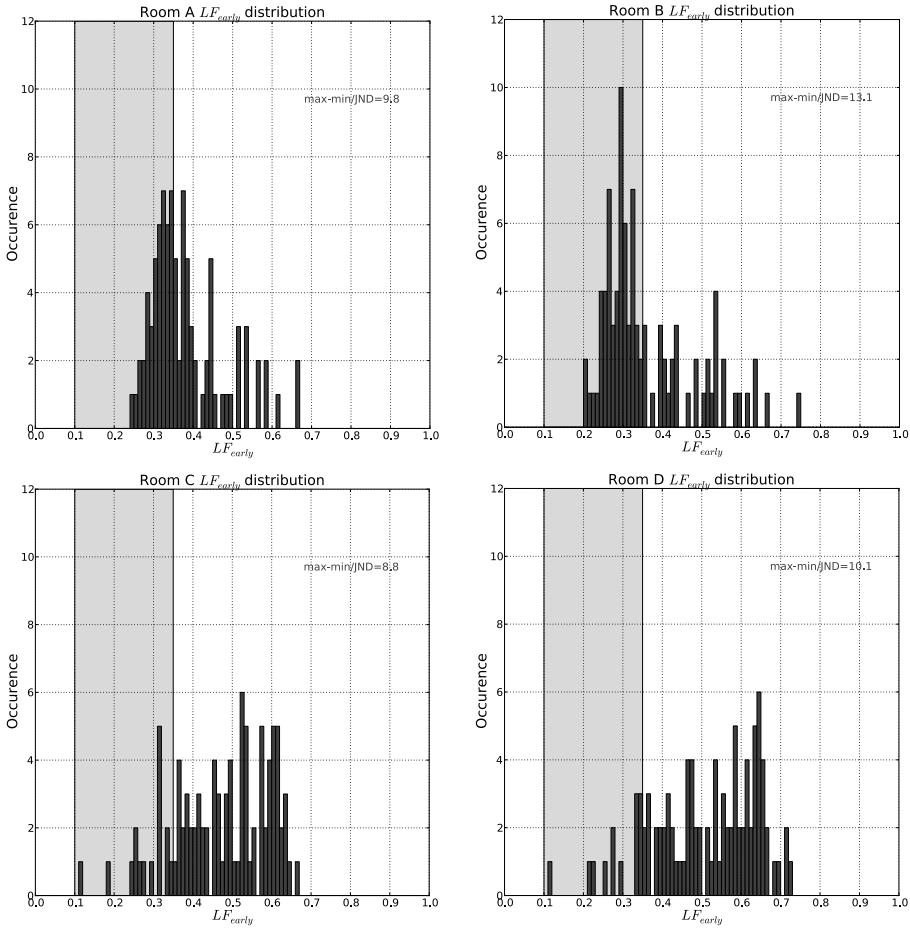

Figure 13.7: Histograms of the distribution of LF_{early} for rooms A, B, C and D.

$$
\begin{aligned}
a_1 &= 1.2 \\
a_2 &= 1.42 \\
a_3 &= 0.04 \quad \text{for} \quad G_{mid} < 4.0 \\
&= 0.07 \quad \text{for} \quad G_{mid} > 5.5 \\
a_4 &= 9 \quad \text{for} \quad EDT < 2.0 \\
&= 12 \quad \text{for} \quad EDT > 2.3 \\
a_5 &= 10 \quad \text{for2.2} \quad \text{sec} \\
a_6 &= 1
\end{aligned}
\tag{13.4}
$$

An important detail to take note of in this formulation is that Beranek is using the average value of each parameter and uses that value to calculate the total subjective preference S. Beranek publishes a series of graphs that show the weighed value of S_i for possible average EDT values. Figure 13.8 shows the graph for S_4, the graph for EDT.

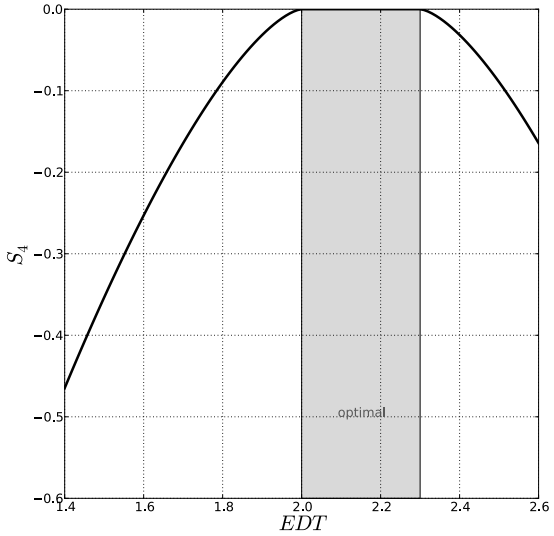

Figure 13.8: Beranek's weight factor Parabola for EDT.

With this formulation, Beranek considers all values inside the preferred range to have equal subjective significance, while values outside of the pre-

ferred range obtain exponentially lower S_i scores. This exponential decay in subjective preference is also present in Ando's 1983 study. He explains this decay and his subsequent use in subjective preference calculations by means of figure 13.9 (a and b) and the following caption:

> "Scale values of subjective preference obtained by the paired-comparison test for simulated sound fields in an anechoic chamber. Different symbols indicate scale values obtained from different source signals (Ando 1983). Even if different signals are used, a consistency of scale values as a function of each factor is observed, fitting a single curve".

(Ando 2007)

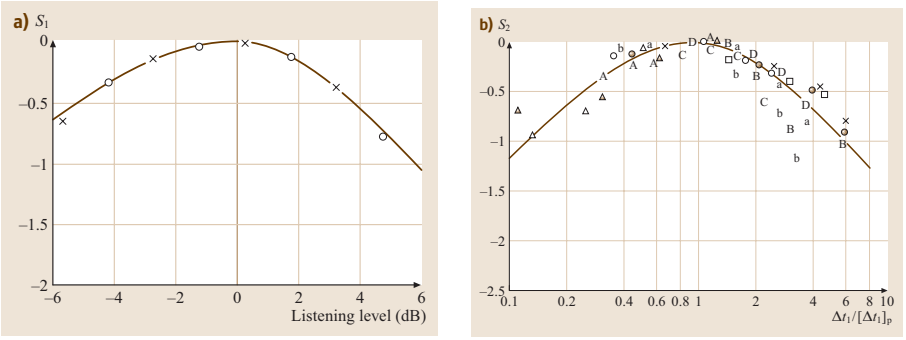

Figure 13.9: Ando's weight factor Parabola for Listening Level LL (a)and Δt_1 (b).

In other words, Ando found that subjective preference decays in an exponential way as parameter values move away from preferred parameter values. This way of quantifying decay gives us an opportunity to measure more accurately the level of satisfaction of any listening position, based on the distance between the measured value and the preferred value and Ando's curve.

In this PhD thesis an equation to study the spatial distribution of sound quality in concert halls based on the difference of measured and optimal values is proposed. Using Ando's theory as employed by Beranek, we sum the weighted differences of optimal and parameter values, for all receivers in

the room. More accurately, we calculate the integral of a function $f_{(i)}$ that is determined by the rooms distribution multiplied by a weighting factor determined by Ando's curve. Figure 13.10 shows the distribution function $f_{(i)}$ for the EDT parameter in rooms A, B, C, and D.

The total distribution score D_i for each parameter i will thus be determined by the following equation:

$$D_i = \int_{-\infty}^{+\infty} f_{(i)} \cdot S_i \, \mathrm{d}x \tag{13.5}$$

where S_i is the subjective weighting curve determined by:

$$S_i = |x_i|^{3/2} \tag{13.6}$$

and where the x_i values are:

$$\begin{aligned} x_1 &= log(EDT/EDT_{pref}) \\ x_2 &= C_{80} - C_{80_{pref}} \\ x_3 &= G - G_{pref} \\ x_4 &= log(LF_{early}/LF_{early_{pref}}) \end{aligned} \tag{13.7}$$

where EDT, C_{80}, G and LF_{early} are the measured parameters values and EDT_{pref}, $C_{80_{pref}}$, and $LF_{early_{pref}}$ are the mid points of the preferred parameter ranges. As already mentioned the G parameter is considered in respect to the source-receiver distance d, so G_{pref} is calculated using Barron's formula (see equation 12.6). The values for S_i can also be expressed by the curves in figure 13.11.

The preceding formulation can be simplified in order to avoid the approximation of the histogram into $f_{(i)}$. The actual values measured in the room can be used in the following set of equations:

$$D_i = \frac{1}{n} \cdot \sum_{i=1}^{n} S_{i,n} = \frac{1}{n} \cdot \sum_{i=1}^{n} (|x_{i,n}|)^{3/2} \tag{13.8}$$

where n is the number of receivers measured in the concert hall. The room that obtains the highest D_i value is considered the room with the most uniform distribution of optimal parameter i values.

If we use equation 13.8 to study C_{80} for rooms A, B, C and D we get different results than those obtained by looking at the percentage of satisfied receivers. Figure 13.12 shows normalized values for both measurement types for C_{80} in our test rooms. The comparison shows that the relationship between these rooms has changed substantially. Room A for example is

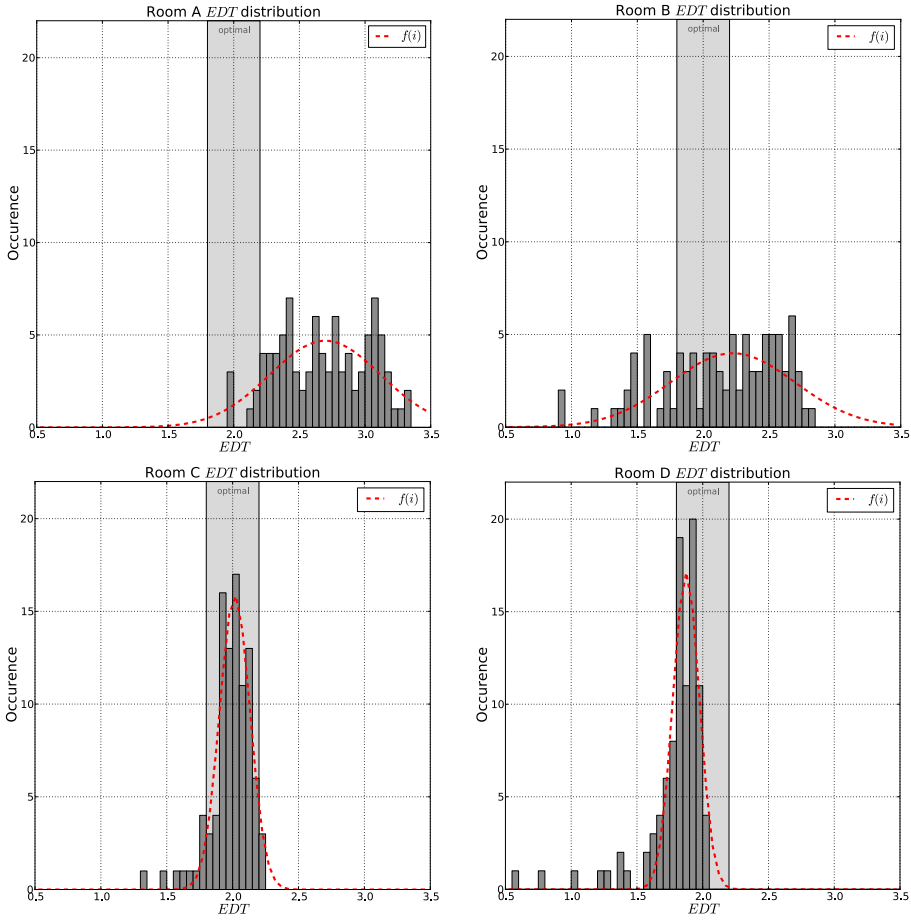

Figure 13.10: Distribution functions $f_{(i)}$ for the EDT parameter of rooms A, B, C and D.

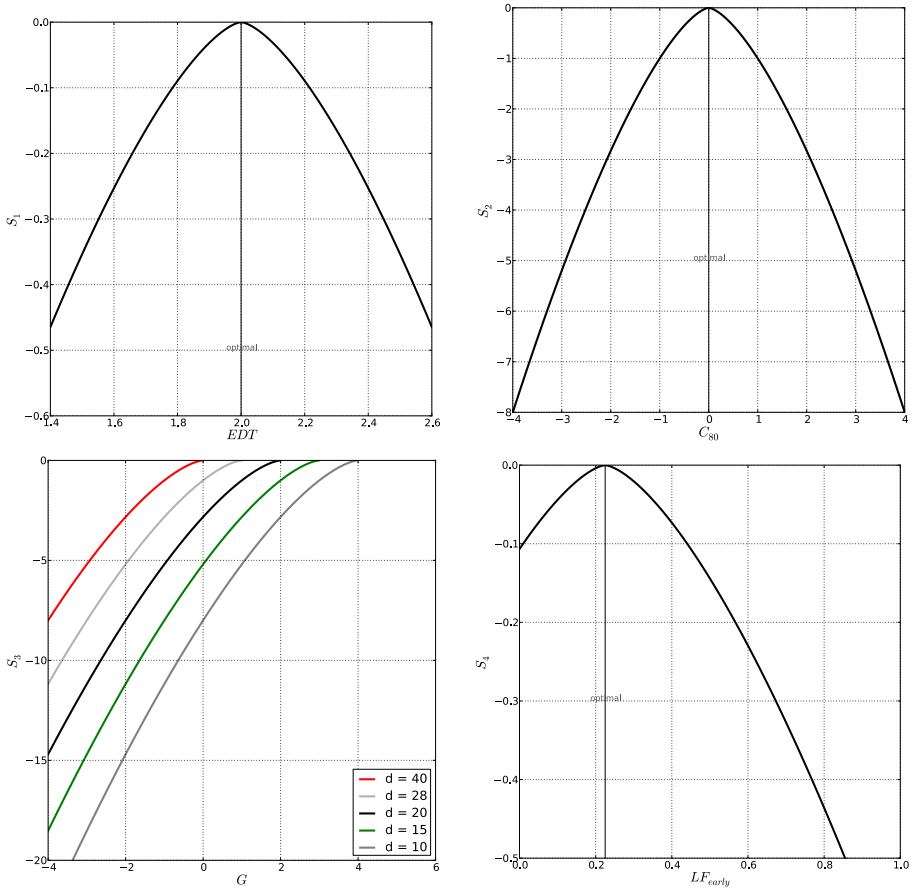

Figure 13.11: Proposed weight factor curve for EDT, C_{80}, G and LF_{early}.

much closer to rooms B and C, gaining a lot of distribution fitness. Room B on the other hand looses distribution fitness in the new measurement. This new measurement seems to better reflect what wee see in the unsatisfied analysis (figures 13.1 and 13.2) and the histograms for C_{80} (figure 13.5).

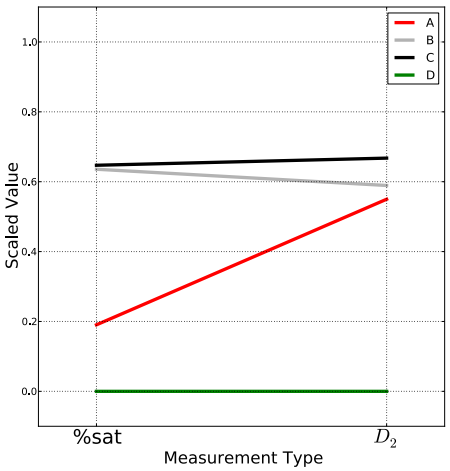

Figure 13.12: Percentage of satisfied receivers for C_{80} and D_2 comparison.

The formulation proposed in this PhD research differs from Beranek's and Ando's in that it takes into account room distribution (all of the measured values in the room) and not just the room average values.

13.2.6 Discussion

When it comes to expressing room parameters in a single value, or just a few numbers we can employ different techniques. While very common, the mean value is appropriate only for Reverberation Times, and not for other parameters that have a greater variation inside the room. The mean value accompanied by the standard deviation is a much better choice, but its difficult to make comparisons based on those numbers if the means are different. It is also not statistically correct to use standard deviations in non-normal distributions.

Comparisons can be made by using optimal values as references. Barron's percentage of satisfied receivers while having advantages lacks information about the unsatisfied receives. We can say that using the percentage of satisfied receivers has the added value of communicating to the designers the extent to which the receivers are inside the optimal range quite clearly. On the other hand the standard deviation is not as clear as to how much improvement it would still need to obtain an acceptable result.

The percentage of satisfied receivers however, fails to inform about the conditions of receivers outside the optimal range. As figures 13.1 and 13.2 suggests, rooms can have high numbers of satisfied receivers at the expense of unsatisfied ones, distributing sound quality unevenly. A new approach is proposed, making use of the difference between measured values from all positions in the room, and weights them according to Ando's theory of subjective preference(Ando 1983).

13.3 Parametric study of concert Hall Types

Klosak and Gade studied the effect of shoebox room proportions (width/length) have in acoustical parameters by means of computer simulations of 24 different rooms (Klosak & Gade 2008). They plotted mean values of several acoustic parameters accompanied by their standard deviations and the 90th percentile. They found that the proportions of the room had a significant influence on the distribution of acoustic parameter values.

Bradley(Bradley 2011) describes four main categories of acoustical parameters: Decay times, clarity measures, sound strength and measures of spatial effects. In this section we will investigate the distribution inside concert halls by means of a parametric study using one parameter from each of these four categories. A large number of computer simulations of concert halls were made for each room typology, and each one of the simulation results was analyzed with the difference weighted sum method described above.

13.3.1 Selection of Types

The most built room type across the last century has been the shoebox, and in recent years the vineyard room has been increasing in popularity(Meyer 2013). This PhD thesis presents a parametric study of the distribution of acoustical parameters in shoebox, fan shaped and hexagonal rooms.

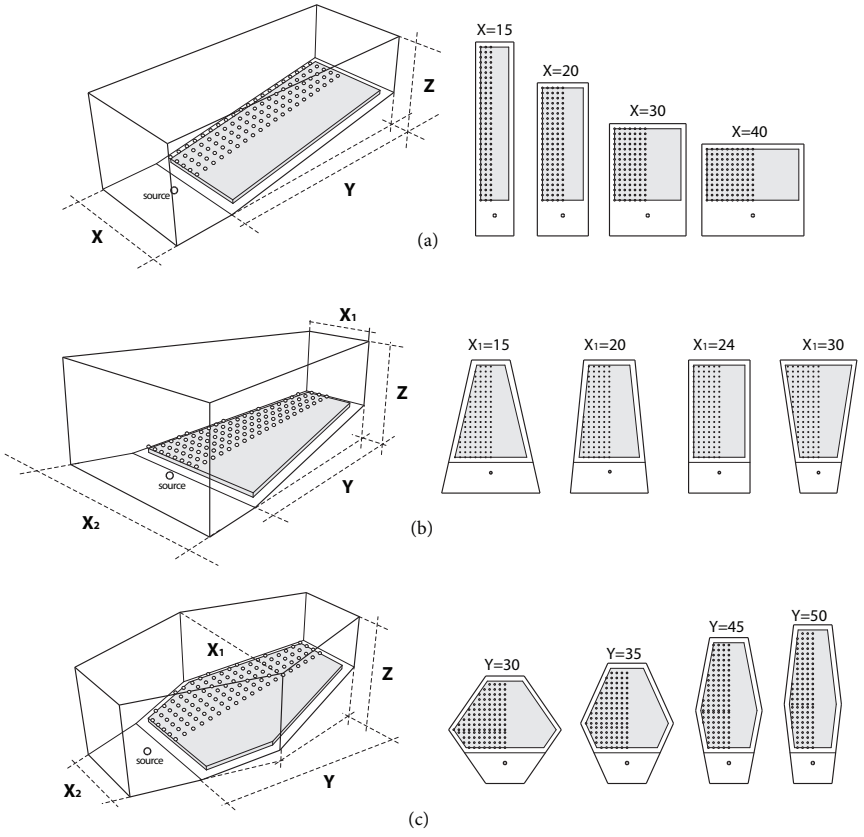

Figure 13.13: Shoebox, Fan and Hexagon geometry parametrization.

Each typology is studied in terms of their form, volume and proportions. The variations in shape are different for each typology and will be detailed bellow, but all the rooms studied have the same audience area, so a comparison of results between room types is also possible. These room types were selected because of their use in concert halls throughout the world, and because their geometry makes it possible to make such a parametric study.

Many variations of each room type will be computationally generated and studied for later comparison. Only the general geometry of the room will be studied, no balconies canopies or surfaces will be included in the simulations. All of the room types will include a 10% inclination in the audience area.

While vineyard rooms are also an important type in today's concert halls, their geometry is far more complicated to study. There are too many variations of vineyards to include in a single study, their geometry is hard to describe by using few variables. For this reason they were left out of this study.

13.3.2 Methodology

Geometry Parametrization

Figure 13.13(a) shows the parametrization of the shoebox room geometry. audience area remains fixed as geometry in plan is changed, Y decreases as X increases. The two geometric parameters that determine the shape of each shoebox room are the height of the room (Z) and the width/length ratio (X/Y).

Figure 13.13(b) shows the parametrization of the fan shaped room geometry. Also in this case audience area remains fixed, so as X_1 increases X_2 decreases. The room length (Y) remains unchanged. The two geometric parameters that determine the shape of each fan room are the height of the room (Z) and the X_1/X_2 ratio.

Figure 13.13(c) shows the parametrization of the hexagonal room geometry. In order to maintain audience area fixed in this type of room the room's length (Y) decreases as the room's width at the center of the room (X_1) increases. The room's width at the ends of the room (X_2) remains fixed. The two geometric parameters that determine the shape of each hexagonal room are the height of the room (Z) and the width (at mid room)/length ratio (X_1/Y).

Type	V_1	Dom	V_2	Dom	Step Size
Shoebox	X	15 to 35m	Z	15 to 25m	1m
Fan	X_1	13 to 35m	Z	15 to 25m	1m
Hexagonal	Y	20 to 50m	Z	15 to 25m	1m

Table 13.1: Parameter domain and discretization for each room type.

Fitness landscapes

The parametric study was done by calculating the acoustic parameters for a series different rooms of varying shape, and comparing results. Since each concert hall typology was parametrized using 2 variables (V_1 and V_2), the different room shapes studied can be expressed as a combination of V_1 and V_2. If we create a grid made up of V_1 in its X axis and V_2 in its Y axis, we can plot the performance of these rooms in the Z axis and create what is known as a fitness landscape. Table 13.1 shows the variable domains for V_1 and V_2 for all room types as well as the size of the variation for each variable at each step.

Acoustical simulation

The acoustical simulations were done with Pachyderm Acoustical Simulation (van der Harten 2011) plugin for Rhinoceros. Pachyderm Acoustical Simulation is a collection of acoustical simulation algorithms for use in Rhinoceros, ranging in purpose from prediction to auralization. Among its features are a growing number of simulation algorithms that can be performed using mesh or NURBS models. Pachyderm combines the source image method with a the ray-tracing technique.

Room materials study

The prime goal of this chapter is to understand the influence of room shape in the distribution of acoustical parameters inside performance spaces. But room shape is not the only factor that affects this issue and it is not easy to study room shape independently. We can understand this difficulty by looking into Sabine's formula *. It teaches us that reverberation times depend on room volume and total absorption area, which in turn depends on the

*see formula 12.1 on page 192

room's surfaces area and the materials of these surfaces. A room's shape affects its volume and the area of its surfaces, so in order to study room shape we would have to keep the materials absorption coefficient fixed. However, keeping absorption fixed would not be sufficient to maintain a fixed total absorption, in order to do so material surfaces would also have to be fixed. This means that, if we want to study the effects of only the room's shape, we would have to use geometries that had the same room surfaces as well as keep materials fixed.

Klosak and Gade studied the effect of shoebox room proportions (width/length) have in acoustical parameters by means of computer simulations of 24 different rooms (Klosak & Gade 2008). They plotted mean values of several acoustic parameters accompanied by their standard deviations and the 90th percentile. They used 3 groups of shoebox rooms that kept room surfaces, materials and volume fixed, consequently also keeping the reverberation time fixed. The only modification between rooms inside each group was the width to length ratio. They reported noticeable changes in acoustical parameters and their distribution inside these rooms.

The study presented in this chapter involves room changes that go beyond the width/length ratio, they also include room volume and total surface area. But in order to do this we need to clarify the influence of the material in sound quality distribution. Figures 13.14 and 13.15 shows two sets of histograms for the distribution of C_{80} in rooms A, B, C and D. The first set (seen in the left column) shows the histograms of the rooms with a fixed absorption coefficient for all of the surfaces in the room excepting the audience. The absorption coefficient for those surfaces in this set was fixed at 10%. The second set of histograms (seen in the right column) show the histograms for the same rooms but with a variable material absorption coefficient. The materials are set in such a way as to keep reverberation time fixed with the changing of the room's surfaces and volume. In other words, the absorption coefficient for these rooms is selected by using the following equation:

$$a_{room,f} = \frac{(\frac{0.161 \cdot V}{RT_f}) - (S_{audience} \cdot a_{audience,f})}{S_{room}} \tag{13.9}$$

where $a_{room,f}$ is the absorption coefficient for frequency f of all the surfaces in the room except the audience area, V is the room volume, RT_f is the desired reverberation time for frequency f, $S_{audience}$ is the surface area of the audience, S_{room} is the sum of all areas of all the surfaces of the room and $a_{audience,f}$ is the absorption coefficient of the audience for

frequency f. For the 500Hz and 1000Hz octave bands $RT_f = 2$ seconds [†].

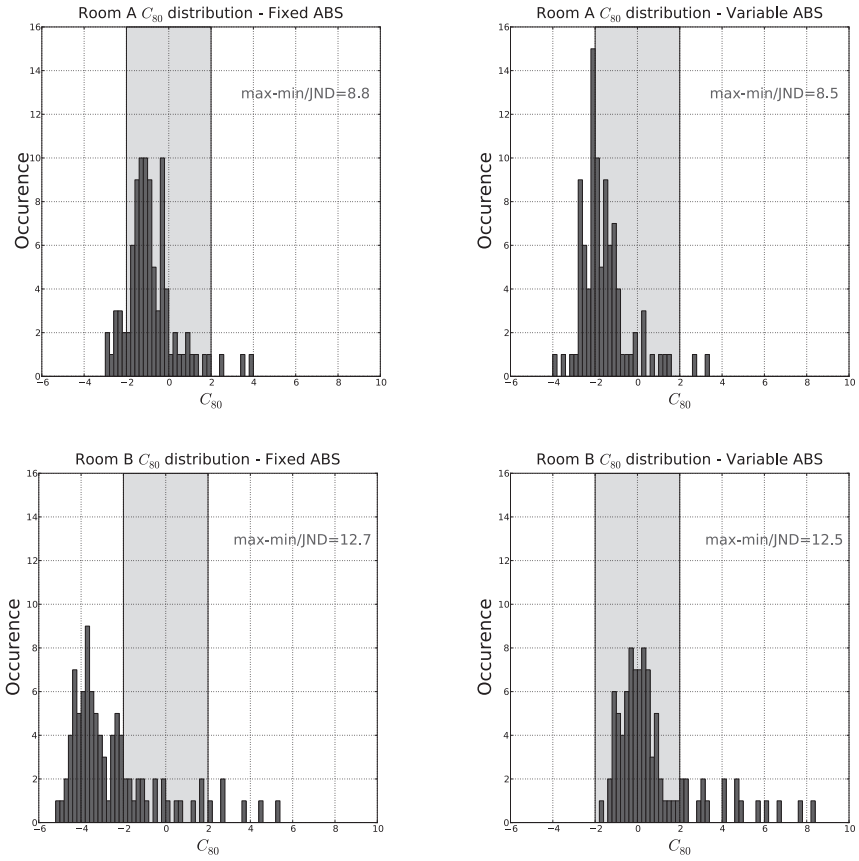

Figure 13.14: Histograms for rooms A and B for C_{80} distribution with fixed and variable material absorption coefficient.

These rooms all belong to the same shoebox parametric model explained above, hence they all share the same rules. Most importantly, in all of these rooms the audience area is kept constant. For these reasons we can say that Rooms A, B, C and D serve as a guide of what is happening with all of the rooms in terms of the material's influence.

[†]This value was taken from (Barron 2009*a*).

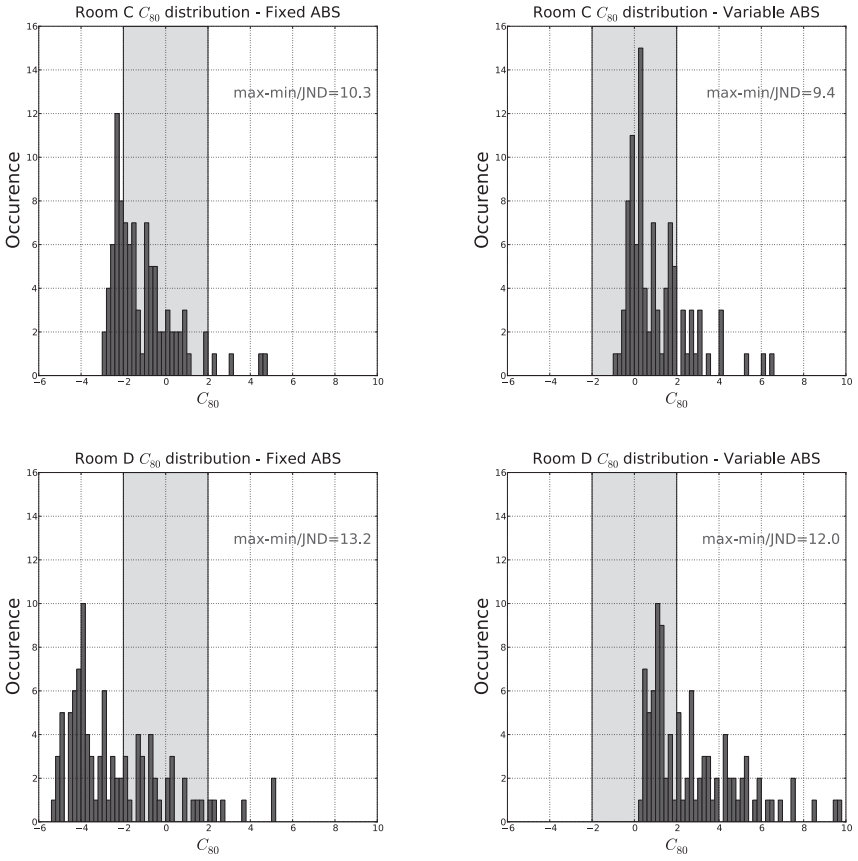

Figure 13.15: Histograms for rooms C and D for C_{80} distribution with fixed and variable material absorption coefficient.

Figures 13.14 and 13.15 is organized in such a way as to have room A with fixed absorption on the left and room A with variable absorption on the right of the same row. This is the same for rooms B, C and D, thus facilitating comparisons. By comparing the histograms on the left with those on the right we can see that the distributions for these two rooms are similar, they have a very similar 90% width to JND ratio. The comparison reveals one important difference, room distributions are traslated from the other as is evident by comparing how they relate to our optimal range. With the exception of room A, all histograms on the right have similar distributions to those on the left but with higher C_{80} values. Room A seems to show no movement and very little variation in width to JND ratio.

The fact that the distribution is very similar tells us that the material has little influence in the distribution of acoustic parameters, but only on their position from optimal values. This is also true for EDT, G, LF_{early} and $T30$ with different degrees. In some cases the influence of material is more present in distribution, but generally speaking we can say that material does not have the largest importance.

This fact should not be completely surprising, given what we know about RT and room shape. Barron (Barron 2009*a*) explains that the most important factors in the determination of RT in a room are room volume and audience area. As we have discussed above, our parametric model keeps audience area constant throughout the variations, including those for rooms A, B, C and D. That leaves only room volume as the determining factor for RT, and leaves out material absorption.

Material selection for parametric study

Having studied the influence of materials in the distribution, and seen how the most important factor is not material but room shape, we can decide wether to use a fixed material absorption or to change material to keep reverberation time fixed. Since material absorption affects not distribution but values in relation to the optimal range, we have to conclude that in order to find the shape that best obtains the best distribution of *optimal* values we need to study the combination of material and shape. For this reason, keeping the material fixed would strongly limit the scope of the study.

In this chapter we chose to change the absorption coefficient of the room's surfaces (with the exception of the audience) using the approach described in equation 13.9. Because this approach keeps reverberation times fixed, we can exclude RT as a parameter to study and concentrate on EDT,C_{80}, G and $LFearly$.

The diffusivity of the room's surfaces also influences the distribution of sound quality. However in this case, since it has little influence on the reverberation time, we decided to keep a scattering coefficient fixed at 50% for the room surfaces, except for the audience. The audience was given a 70% scattering value. These numbers have been taken from (Lam 1996).

13.4 Case Study 6: Parametric Shoebox, Fan and Hexagon

Case study 6 is the typological parametric study developed with the method described above. The subject of this case study are the 3 room typologies presented above. In this case, the search process is not done via a MOGA but with an exhaustive search algorithm and the fitness landscape technique. This is due to the fact that this problem is subdivided into room types, and each room type has only 2 variables. Hence an exhaustive search within normal variable domains is not too time consuming, and it allows us to better understand and diagram the problem.

The parametric study results are studied in two ways:

- Comparisons within room types. This is a comparison of rooms in the same type, we study the incidence of the room variations in shape has on the distribution of quality for all four of the acoustic objective parameters.

- Comparisons between types. This is a comparison of the distribution of acoustic parameters between the 3 different room types. The purpose is to examine the particular qualities that make each type better or worse in each acoustic parameter distribution.

Each comparison has its own representation method.

13.4.1 Comparison within room types: Fitness landscapes

The concept of the fitness landscape was explained in section 10.1.3. In this comparison we use a fitness landscape for each acoustical parameter and each room type.

Shoebox Rooms

Figure 13.16 shows the fitness landscapes for EDT, C_{80}, G and LF in the shoebox room type. As shown in table 13.1, the shoebox rooms have two variables: x_1 that represents the room width, and x_2 that represents the room height. All landscapes thus have the x_1 variable in the x axis and x_2 in the y axis. The z axis of the landscapes vary, each one indicates a different acoustic parameter. The first one (upper left) shows D_1, the second (upper right) shows D_2, the third (lower left) shows D_3 and the fourth shows D_3 , all calculated with equation 13.8.

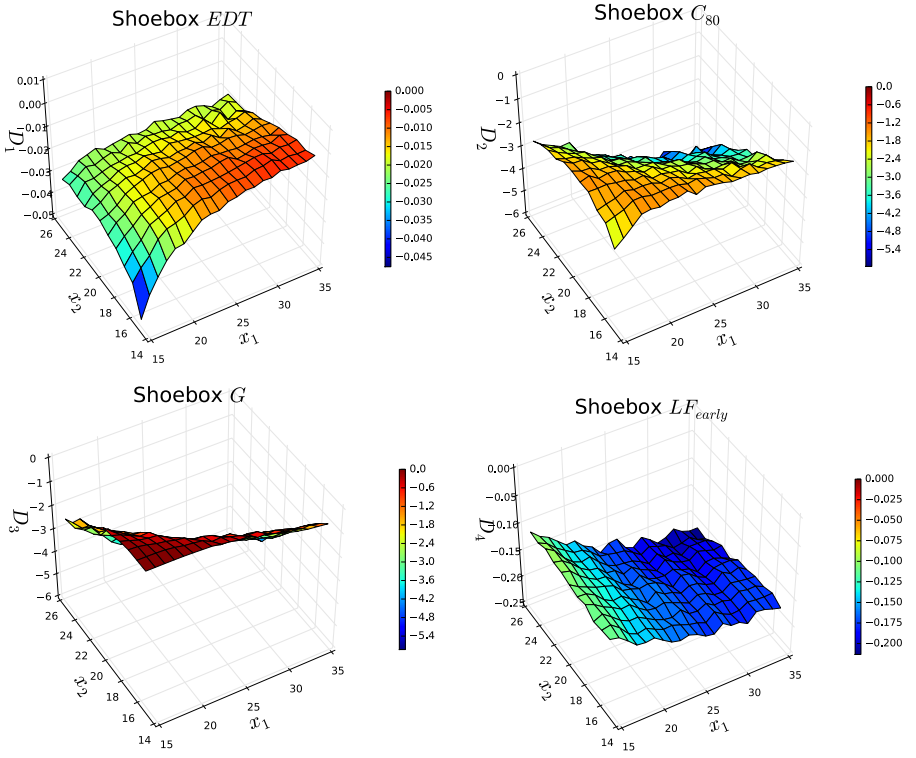

Figure 13.16: Fitness landscapes for the shoebox room type for EDT, C_{80}, G and LF_{early}.

Shoebox rooms show sensitivity to both room width/length ratio and

height when it comes to EDT, C_{80} and G, while LF_{early} seems to be only affected by the width/length ratio. This is a reasonable result since LF_{early} is the only parameter that is completely independent of reverberation.

C_{80} and G have the highest values when rooms are long, narrow and not very high, while EDT shows a preference towards short,wide and also not very high rooms. The overall trend shown in the landscapes for C_{80} and G seems to be very similar, but it can be argued that for different reasons. In the case of G the preference can be explained by the room volume, G values tend to be lower as volume increases. And since this parameter has no maximum optimal value, the higher the G the better the D_3. In the case of C_{80} this can be explained by the presence of higher early reflections when the rooms are narrow. This is perhaps most important in our case study because there are no other surfaces in the room that provide early reflections, apart from the sidewalls and the ceiling, there are no canopies or balcony overhangs. In the absence of early reflections C_{80} values tend to be low, and EDT values tend to be high (Barron 1995). That also explains why EDT preference goes towards wider rooms. Taller rooms have too much reverberation, and therefore, too long $EDTs$ for our optimal range (1.8-2.2s).

Early Lateral Fractions are at their highest D_4 values when the rooms are narrow, regardless of room height.

Fan shaped rooms

Figure 13.17 shows the fitness landscapes for EDT,C_{80}, G and LF in the fan shaped room type. In the case of the fan shape room, table 13.1 shows that the variables for the fan are: the room's width at the end of the room, and the room's height. All landscapes thus have the x_1 variable in the x axis and x_2 in the y axis. In the same way as the shoebox example, the z axis represents distribution values for our four acoustical parameters calculated with equation 13.8.

It is important to notice the way these room's geometry changes in plan when x_1 increases. When $x_1, 24$m is low, the room is an inverted fan, when $x_1 = 24$m it is a shoebox, and when $x_1 > 24$m it is a fan shaped room. This is shown in small plan views in figure 13.13(b).

The most important variation this progression in the angle of the sidewalls from the point of view of the sound source. When the room has a regular fan shape the sidewalls open up from the stage towards the room, when it is an inverted fan the walls are closed towards the room. An open angle towards the room produces a higher number of early reflections arriving

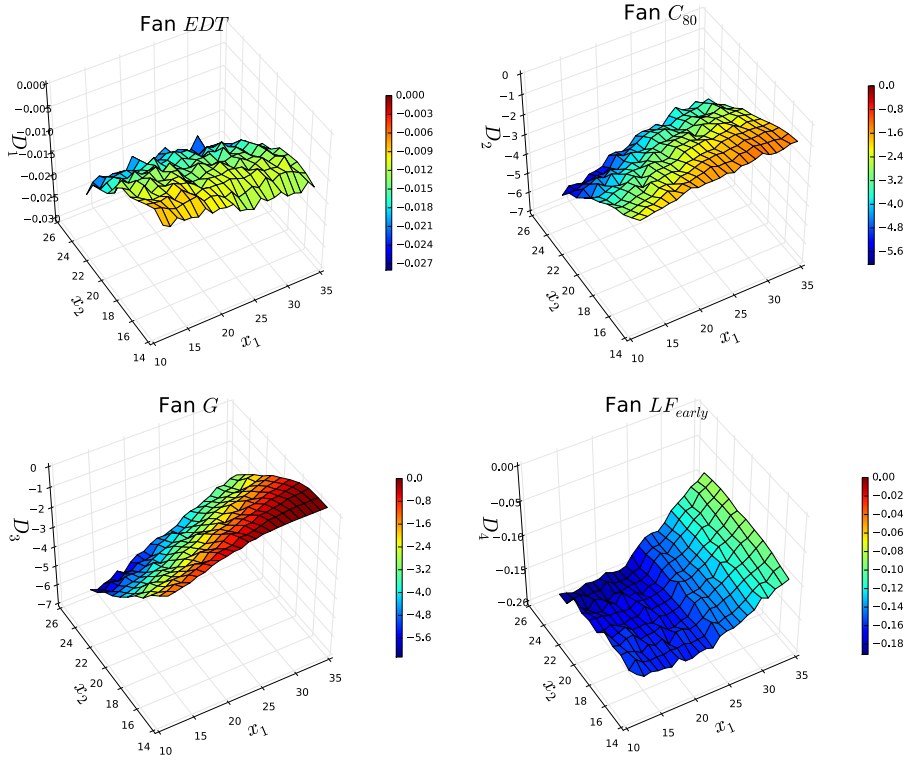

Figure 13.17: Fitness Landscapes for the Fan shaped Room Type for EDT, C_{80}, G and LF_{early}.

the audience. While a closed angle is synonymous with higher reverberation. This behavior is shown in figure 1.3 on page 23. It shows the spatial distribution of the G parameter in 4 variations of hexagonal room with equal room height. High G values are represented in blue and lower ones in red. We can see that an open angle around the stage increases G values in the last rows of the room. We can also see that parallel sidewalls around the stage have the opposite effect, regardless of the angle of the sidewalls around the audience.

This behavior explains the results obtained in this parametric study of the fan shaped rooms. Room height x_2 also has a big importance in the results of some parameters. D_2 and D_3 values are at their highest when an open angle is present around the stage and the room is low, showing little contrast between C_{80} and G (as seen in the shoebox example). EDT seems to have a lower sensitivity to the room shape in plan than it has on room height, however, we find the highest D_1 values when the inverse fan is present and the room is low. This is consistent with Barron's explanation on $EDTs$ (Barron 1995) and the fact that inverse fans have lower early reflections.

Room height has a low but present incidence on LF_{early} values, and the highest D_4 values are found when room is a tall and open fan.

Hexagonal Rooms

Figure 13.18 shows the fitness landscapes for EDT, C_{80}, G and LF in the hexagonal room type. The two variables for this room type (seen in table 13.1) are the room length x_1 and room height x_2. These are the two variables plotted in the x axis and y axis of the landscapes in figure 13.18. As usual the z axis describes D_i.

Also in this case the variation in plan is important to understand the results. As seen in figure 13.13(c), as room length increases, room width at the middle of the room decreases to maintain audience a fixed area. Room withs at both ends of the room are always fixed. This means that sidewall angles in plan vary significantly as x_1 increases. In this case there is never a closed angle from the stage towards the audience, as was the case in the fan shaped rooms. The angle becomes closer to parallel sidewalls as the room length increases, but never getting to the point of becoming parallel.

Results in this study seem to be related in good measure to that movement in plan, showing a higher number of early reflections and a higher G when the room becomes narrower and sidewall angles become more closed, but never flat. Room height also has an important role in the results of all

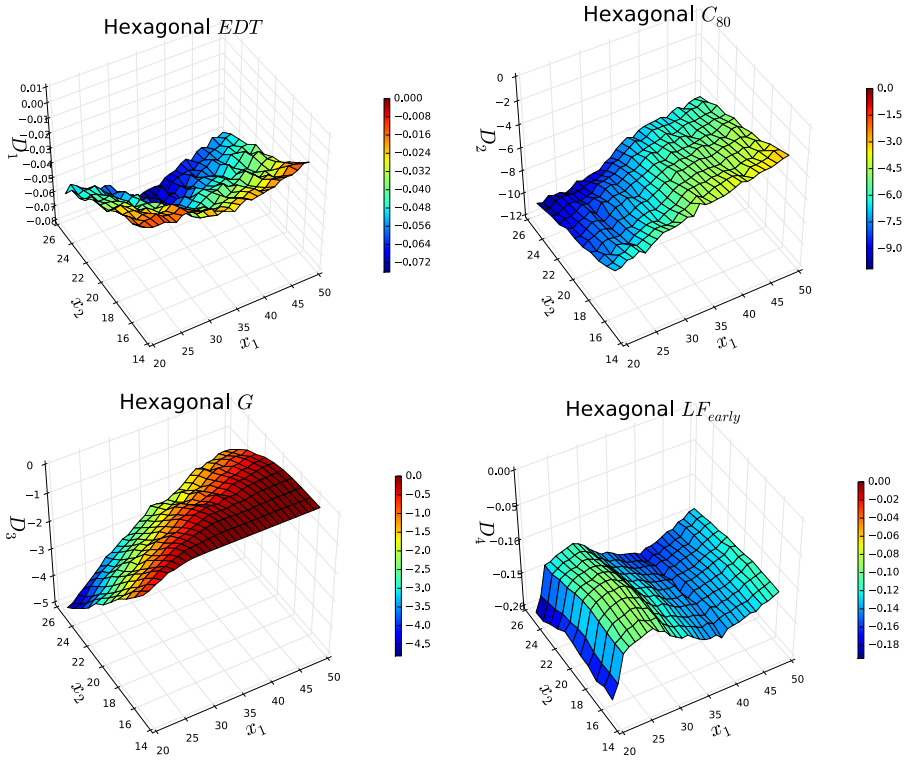

Figure 13.18: Fitness Landscapes for the Hexagonal Room Type for EDT, C_{80}, G and LF_{early}.

parameters with the exception of D_4. As seen in the previous types, D_2 and D_3 values seem to be very much related.

D_1 results show an interesting trend in plan. D_1 values tend to be high either when x_1 values are low or high, but not in mid values. D_1 values are lowest when the rooms are high, but they are also low when x_1 are close o 35 meters. Shoebox rooms have high D_1 values when they are very wide, this can also explain why they are high when rooms are wide in the hexagonal rooms. High D_1 values when x_1 values are high are harder to explain. Results suggests that rooms in x_1 mid range that are not ideal, they seem to have too little lateral reflections but not a high reverberation, while narrow hexagonal rooms regain lateral reflections and reverberation seems to be near optimal.

Also in this case, D_4 values are almost unrelated to room height, they vary only with x_1 values. As is the case with D_1, D_4 numbers are highest in two different sets of rooms. When x_1 is close to 25 and 50 meters, D_4 numbers are high. The D_4 landscape suggests that a good lateral energy is achieved either in very narrow rooms (as seen in the shoeboxes) or in rooms that have an optimal opened angle around the stage (as seen in the fan shaped rooms). Interestingly, when the room is too wide, the angle around the stage is of no help to improve lateral energy and D_4. This could also be related to the angle around the audience, but with a lesser degree of importance.

13.4.2 Comparison between types: Pareto fronts

A more direct comparison between the different types can be seen by studying their Pareto fronts. Since all room types were studied with the same objective functions (D_1,D_2,D_3 and D_4), we can plot an objective space containing all of the room types, and in the objective space, single out the non-dominated individuals. Since there are 4 objective functions, it is not possible to have a single graph representing all functions, objective spaces will be shown in pairs of functions.

Reverberation vs. Clarity

Figure 13.19a shows the Pareto fronts of all 3 room types for the EDT and C_{80} parameters. We can see that shoeboxes have the highest D_1 values and both shoeboxes and fans have high D_2 values. Hexagonal rooms have lower values for both D_1 and D_2.

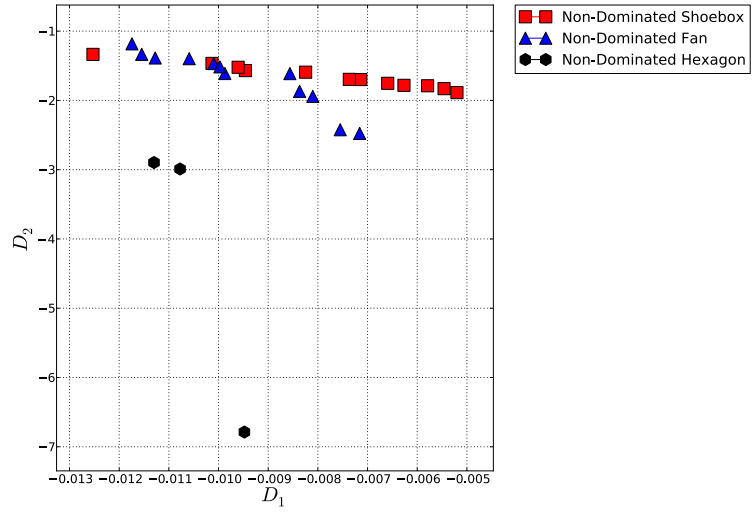

(a) EDT vs. C_{80}

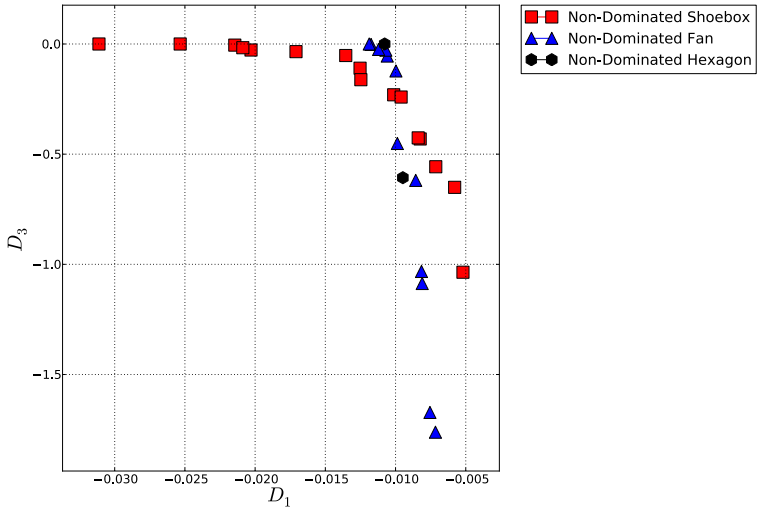

(b) EDT vs. G

Figure 13.19: Pareto Fronts comparisons of the shoebox, fan shaped and hexagonal rooms.

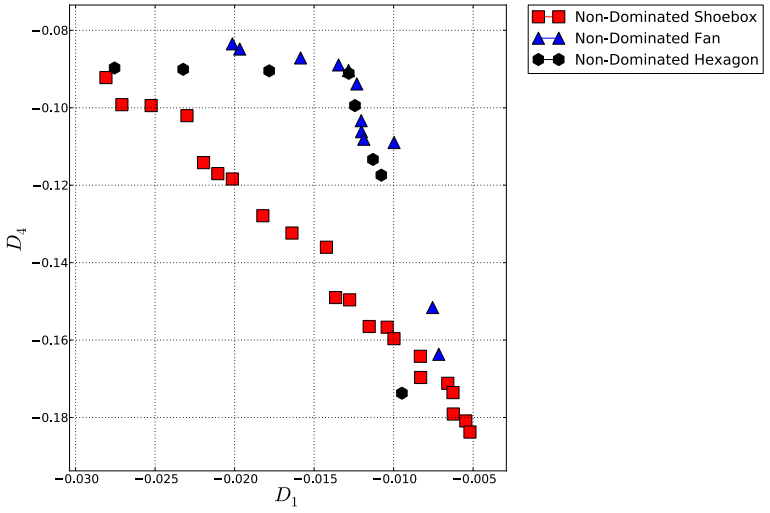

(a) EDT vs. LF_{early}

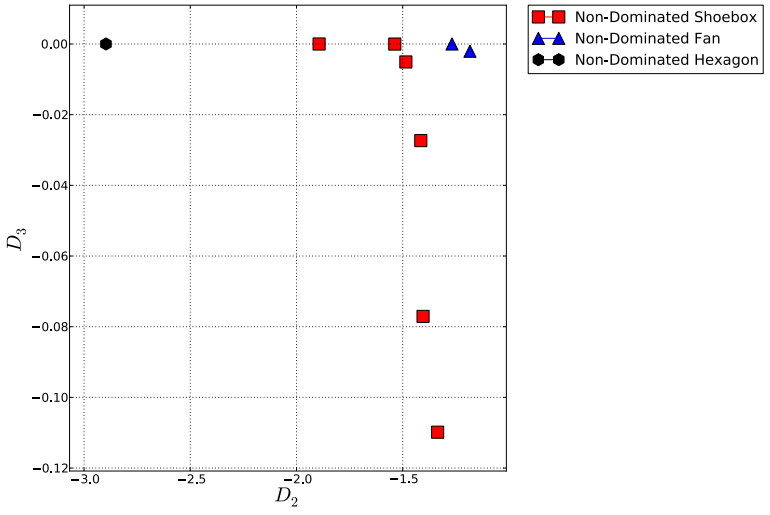

(b) C_{80} vs. G

Figure 13.20: Pareto Fronts comparisons of the shoebox, fan shaped and hexagonal rooms.

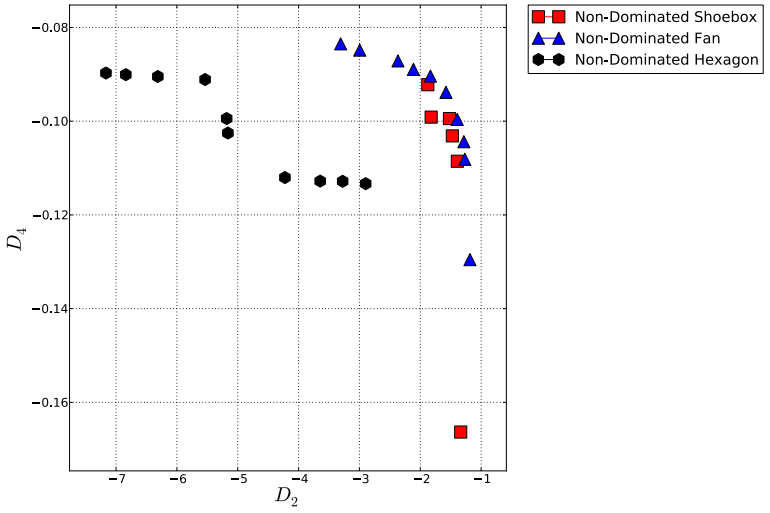

(a) C_{80} vs. LF_{early}

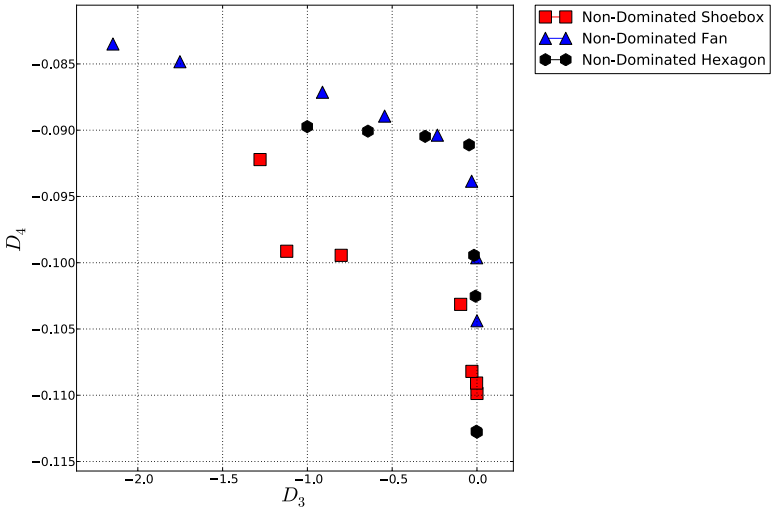

(b) G vs. LF_{early}

Figure 13.21: Pareto Fronts comparisons of the shoebox, fan shaped and hexagonal rooms.

There is contrast between D_1 and D_2, especially in the shoebox and fan shaped rooms. As we saw before, hexagonal rooms have two separate group of solutions with high D_1 values. This is visible also in this figure. Shoebox rooms seem to have a more continuous Pareto Front.

If we had to select a room type based on D_1 and D_2 we would surely not choose the hexagonal type, but between the shoebox and the fan, the choice is not clear. There is a group of shoebox and hexagonal rooms that are non-dominated between each other.

Reverberation vs. Sound Strength

Figure 13.19b shows the Pareto fronts of all 3 room types for the EDT and G parameters. All 3 room types have individuals with a perfect D_3 value ($D_3 = 0$. This means that those rooms have G values that are all above Barron's minimum G curve. However, the highest values for D_1 are found in rooms that do not have a perfect D_3 score. Hence there is some contrast in this objective space, especially so for shoebox and fan shaped rooms.

As seen in the previous comparison, D_1 values are highest among shoebox rooms, but some of them are dominated by fan and hexagonal rooms on the basis of D_2. There seems to be more solutions with a good compromise between D_1 and D_2 in fan shaped rooms, some of these are inverse fans.

Reverberation vs. Lateral Fraction

Figure 13.20a shows the Pareto fronts of all 3 room types for the EDT and LF_{early} parameters. Most shoebox rooms have considerably lower D_4 values than hexagonal and fan shaped rooms. This seems to suggests that good lateral energy distribution is most present when sidewalls are not parallel. Only very narrow shoeboxes have good D_4 values, but they do not have high D_1 values.

Pareto front shapes in this case are almost orthogonal for hexagonal and fan shaped rooms, indicating little contrast, especially when compared to shoeboxes, they have a linear and almost 45 degree Pareto front. This shows that there is little possibility of achieving a good compromise between D_1 and D_4 in the shoebox type.

Clarity vs. Sound Strength

Figure 13.20b shows the Pareto fronts of all 3 room types for the C_{80} and G parameters. This graph shows very little contrast between these two

functions. This behavior was already seen in the fitness landscapes for all three room types. Many rooms in all types have a perfect D_3 score. In this case, those rooms with perfect D_3 scores also include the best D_2 rooms (especially in the fan shaped and hexagonal rooms), further confirming the lack of contrast between these two functions.

This direct Pareto comparison shows that fan shaped rooms dominate all other types. Fans that are open towards the room and have a short height seem to have better distributions of C_{80} and G optimal values than all other rooms in this case study.

Clarity vs. Lateral Fraction

Figure 13.21a shows the Pareto fronts of all 3 room types for the C_{80} and LF parameters. This graph shows that in all room types these two functions are contrasting, perhaps more evidently so in fan shaped rooms. The fan type contains both the best performing room for D_2 and for D_4. Moreover, the Pareto optimal rooms in the fan type dominate all other rooms from the shoebox and fan shaped types. In other words, a Pareto Analysis of all types for D_2 and D_4would place only fan shaped rooms in the front.

Shoebox rooms are generally better at distributing optimal C_{80} values that the hexagonal shaped rooms and they have very similar values when it comes to lateral energy. Therefore we see shoebox rooms dominate hexagonal rooms in this pair of functions.

Sound Strength vs. Lateral Fraction

Figure 13.21b shows the Pareto fronts of all 3 room types for the G and LF_{early} parameters. These two functions show contrast, in all three types there seems to be an almost orthogonal relationship between D_3 and D_4. We can see that the rooms that best distribute lateral energy, and therefore have higher D_4 values, are not the ones with a perfect D_3 score.

Reverberation, Clarity, Sound Strength and Lateral Fraction

The previous comparisons and Pareto fronts were made by considering pairs of objective functions. They help us understand the relationship between these functions and the three room types in great detail. But we are also interested in considering all fitness functions at the same time. While it is not possible to visually represent the Pareto front shape resulting from considering all functions in a four function problem such a this one, we can

still study the Pareto front in other ways. Figure 13.22 shows the shape of the rooms in the Pareto front for the four fitness functions. The following table shows the room type and x_1 and x_2 values for the Pareto rooms:

Shoebox		**Fan**		**Hexagonal**	
X_1	X_2	X_1	X_2	X_1	X_2
15.0	21.0	13.0	16.0	27.0	15.0
25.0	15.0	14.0	16.0	28.0	15.0
25.0	16.0	15.0	15.0	48.0	15.0
26.0	15.0	18.0	16.0	49.0	15.0
26.0	16.0	19.0	15.0		
27.0	15.0	19.0	16.0		
28.0	15.0	21.0	15.0		
28.0	16.0	27.0	15.0		
29.0	15.0	29.0	16.0		
30.0	15.0	30.0	15.0		
31.0	15.0	30.0	16.0		
31.0	16.0	31.0	16.0		
32.0	15.0	32.0	16.0		
33.0	15.0	33.0	16.0		
34.0	15.0	33.0	17.0		
35.0	15.0	33.0	18.0		
13.0	15.0	34.0	15.0		
		34.0	16.0		
		35.0	15.0		
		35.0	16.0		
		35.0	17.0		
		35.0	18.0		
		35.0	19.0		
		35.0	20.0		
		35.0	22.0		
		35.0	23.0		

We can see that the Pareto front is comprised of rooms in all three types. Fan shaped rooms are the most present in the Pareto front, followed by shoebox, and then we see just a few hexagonal rooms. We can also see that most Pareto rooms are low. Rooms from 15 to 17 meters in height comprise about 90% for the front, rooms higher than 17 meters are mostly dominated rooms.

The shoebox rooms that belong to the Pareto front are mostly wide and mid width rooms, there are only two very narrow and long rooms. We saw

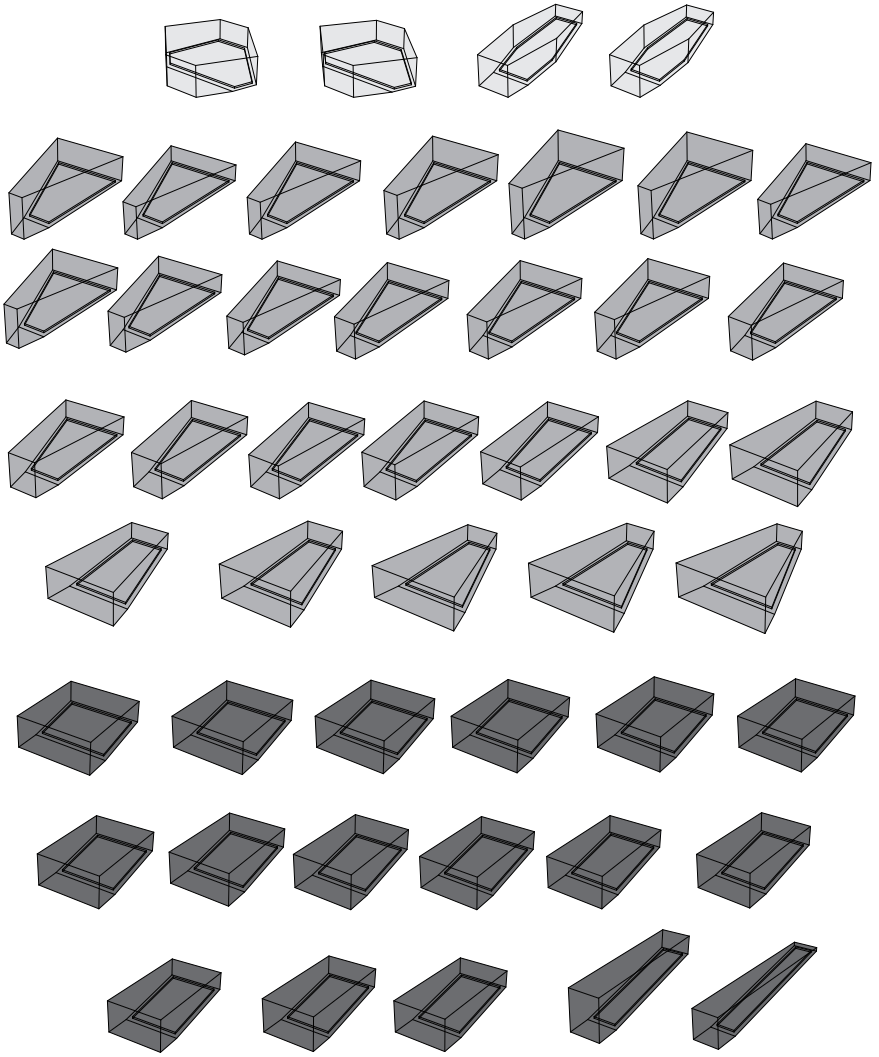

Figure 13.22: Pareto front rooms for the four fitness functions D_1, D_2, D_3 and D_4. Shoebox rooms in dark gray, fan shaped rooms in medium gray and hexagonal rooms in light gray.

above that wide shoeboxes have high D_1 values, and have the fairly high D_2 values as well. Most of them range from 25 to 35 meters in width, meaning a variation also in length (from 50 to 40 meters). These are quite significant differences in plan between rooms.

Fan shaped rooms also vary greatly in plan. Most rooms in this type are regular fans, but there are seven inverse fans in the Pareto front. The most significant difference between the fan rooms in the front is the angle between their sidewalls. Inverse fans have a place in the front thanks to their high D_1 values, while regular fans have very high values in all other functions.

The are four hexagonal rooms the front, two of them are very wide with very open sidewalls, the other two are very narrow, with nearly parallel sidewalls. These two groups correspond to the two groups seen in the fitness landscapes, they have high D_1 and D_4 values.

13.5 Conclusions

Case study 6 presents a parametric study of three concert hall types by means of their distribution of acoustic objective parameters. Distribution of acoustic quality is studied with the method described in chapter 13. The most significant geometrical aspects of three concert hall types are parametrized into three parametric models. These parametric models do not comprise all of the possible variations within these concert hall types. Since only two parameters were used to describe each room type, not all variations of the concert hall geometry were included.

Fitness landscapes and Pareto fronts were plotted from the distribution analysis performed on all three concert hall types. A comparative analysis of room types is made from these figures, and some specific geometrical attributes important to sound quality are derived.

Results show that a particular set shoebox, fan and hexagonal shaped rooms have distinct advantages over all other rooms in the study. The information provided to us by this search process would be of fundamental importance if we were to proceed with these study in a design process. The information obtained by this study could be interpreted in four ways in order to proceed:

- A shoebox from the Pareto set is selected and its acoustic distribution is further improved by including other features in the room.
- A fan shaped room from the set is selected and further developed.

- An hexagonal room from the set can be chosen and further developed.
- A more detailed study of all three types is carried out including other variables or different parametric models.

The first possibility is the selection and further development of the shoebox room. If we look at the values shown in the objective spaces comparisons for the shoebox, we can see that the shoeboxes are most deficient when it comes to D_4 and D_2. It could be argued that by selecting a narrow shoebox, and studying sidewall modifications (such as side balconies or reflectors) improvements to D_4 and D_2 could generate an optimal room.

The second possibility is the selection and improvement of a fan shaped room. In this case the most important improvement necessary for the fan rooms is their D_1 values. Reverberation can be improved by slight modifications in the room materials, especially in the audience seats. Also, a furtter refinement of the room dimensions, leading to higher volumes can also improve reverberation without dramatic changes to other distribution values.

The third possibility involves the selection of an hexagonal room. Narrow hexagonal rooms are the ones with the highest values in their type for all functions. They also rank very highly when compared to all types when it comes to D_3 and D_4. Interestingly, this type needs improvement both in reverberation and clarity. It is therefore difficult to visualize a clear step for improvement, but a study in greater detail in the sidewall angles around the stage might be good start.

The fourth possibility is that of creating a new search process with different, perhaps more detailed parametric models, using the information obtained in this study. For example, there is a way of significantly improving the performance of hexagonal rooms by including more control over sidewall angles and room width. As we saw in the fitness landscapes, hexagonal rooms were too wide or too open in some instances. A parametric model that works on these variables can probably obtain better results, giving designers more options. Different angles for stage and audience sidewalls are a great possibility of hexagonal rooms. This was not included in the present parametric study.

14

Acoustic simulation of complex shapes in concert halls

Ray tracing acoustic simulation (Krokstad et al. 1968) has been used for predicting the room impulse response for a number of years and represents an important method that is present in most of acoustic simulation packages.*

When it comes to describing the geometry of curved surfaces commercial acoustic simulation software depends on their discretization into small planar segments. This is partly because planar segments are needed to use the Image Source Method, partly because other more precise geometrical models are not easily implemented. These kind of segmented surfaces are sometimes called meshes, and they are the kind of surface geometry contained in DWG and DXF files, popular formats used for importing of geometry into commercial acoustic simulation software.

The advent of advanced computational geometry, in particular the use of NURBS, give us the possibility to better represent free-form complex and curved geometry. This presents the opportunity to significantly improve raytracing simulation models by accurately representing curved geometry, as has been recommended by researchers in the past (Kuttruff 1993, Vercammen 2010, Mommertz 1995). This chapter conducts a comparison of simulations done with and without the use of NURBS for a series of curved surfaces in order to understand the potential of this new possibility. In so doing we can demonstrate that with NURBS geometry we can correctly cal-

*The contents of this chapter were published in the proceedings for the AIA-DAGA symposium on acoustics in Merano in 2013 (Méndez Echenagucia, Astolfi, Shtrepi, van der Harten & Sassone 2013*c*)

culate reflection angles for curved surfaces of any kind, without resorting to discretizations. We also show, as previously seen in (Kuttruff 1993, Vercammen 2010), that with raytracing algorithms, using mesh geometry can that give out erroneous results, especially with regards to concave surfaces, resulting in the failure to detect sound concentrations.

14.1 Sound reflection from convex surfaces

In order to study the potential of NURBS surfaces in acoustic raytracing simulation, we turned to theoretical studies (Kuttruff 1993) and (Vercammen 2010) of sound fields of curved surfaces and compare their findings to results obtained with a NURBS raytracing acoustic simulation algorithm developed for this PhD thesis. A cylinder, a sphere and an ellipsoid serve as examples of concave surfaces studied in these research papers, and they are reproduced here as described bellow. Figure 14.1 shows the geometric and acoustic setup for all three geometry cases.

14.1.1 The Image Sources Method

In the case of Image sources, a number of flat segments that gives a good approximation to the correct sound pressure in the centre can be estimated (Kuttruff 1993, Vercammen 2010, 2012). This number of segments is frequency dependent and can be rather large, especially in the case of double curvature surfaces. In this chapter the image source method will not be considered, since this method is not possible with NURBS, due to the fact that there are an infinite number of image sources, and no flat segments.

14.1.2 The raytracing NURBS simulator

The studies described in (Kuttruff 1993, Vercammen 2010, 2012) call for a first order raytracing simulation of concave perfectly reflective surfaces. Such an algorithm was written with the use of NURBS geometry, inside Rhinoceros.

As explained above, Rhinoceros is a commercial Computer Aided Design package that is used in various fields, particularly those who employ complex curved surfaces, as it is capable of representing and operating on NURBS geometry. Rhinoceros also allows the user to customize its functionality by creating commands by calling a series of Rhinoceros functions. This is done through scripts that can be written in Visual Basic or Python programming

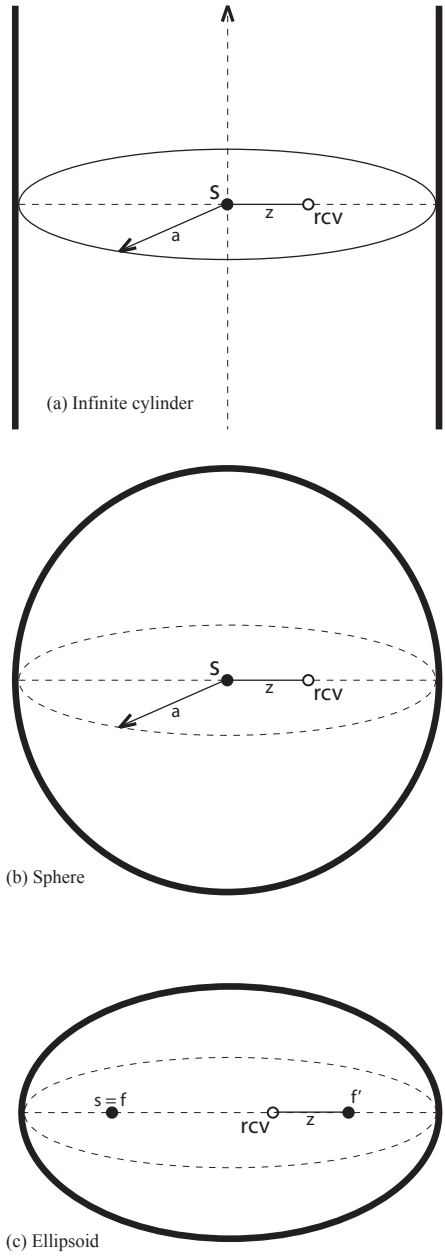

Figure 14.1: Cylinder (a), Sphere (b) and Ellipsoid (c) Geometry and acoustic setup for NURBS and Mesh raytracing analysis.

Languages. In this case a Python class containing a series of functions was written.The class of functions is able to cast rays into NURBS or mesh geometry and to plot their path, as well as create spherical receivers that can detect the energy inside each ray. The sound power in each ray can be described by:

$$P_i = P/N \qquad \text{(W)} \tag{14.1}$$

where P_i is the power of the i_{th} ray, P is the source power and N is the number of rays (Cingolani & Spagnolo 2005). The developed ray tracer does not take air attenuation or absorption from reflections into account, since this is not a part of this study, and the source is always considered to be omnidirectional. In (Cingolani & Spagnolo 2005) we find that the ray power detected by the source can be normalized in relation to the ray length inside the receiver volume. In this case the sound power in each ray will be:

$$P_{i,m} = \frac{l_{i,m}}{D_m} \cdot \left(\frac{P}{N}\right) \qquad \text{(W)} \tag{14.2}$$

where $P_{i,m}$ is the power of the i_{th} ray in the m_{th} receiver, $l_{i,m}$ is the i_{th} ray segment inside the m_{th} receiver volume, D_m is the receiver diameter. The intensity at the receiver will be:

$$I_i = \frac{P_{i,m} \cdot \Delta t \cdot c}{V_m} = \frac{P_{i,m} \cdot l_{i,m}}{V_m} \qquad \text{(W/m}^2\text{)} \tag{14.3}$$

where V_m is the m_{th} receiver volume, c is the sound speed and Δt is travel time of the ray inside the receiver volume (Xiangyang et al. 2003, Vercammen 2012). From the sound intensity we can calculate the mean squared sound pressure with:

$$p^2_{rms} = \rho c \sum_{i=1}^{N} I_i = \rho c \sum_{i=1}^{N} \frac{P_{i,m} \cdot l_i}{V_m} \tag{14.4}$$

where ρ is the air density. Since no absorption or attenuation is considered in the concave surfaces examples in (Kuttruff 1993, Vercammen 2010, Mommertz 1995) the ray tracer developed for this PhD thesis makes no considerations regarding sound frequencies. All of the simulations in this chapter assume conditions in which the rules of geometrical acoustics can be applied.

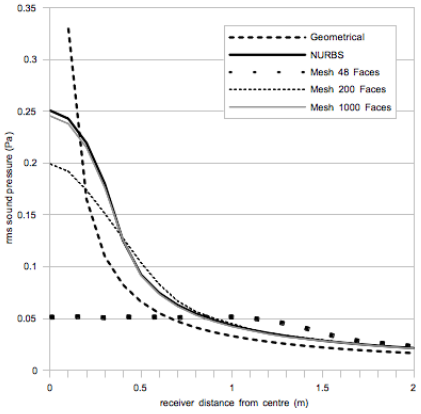

Figure 14.2: Infinite Cylinder with 10 meter radius - mean squared sound pressure in relation to receiver distance from cylinder centre. All receivers with a 0.8 m diameter.

14.2 Cylinder Study

Kuttruff describes in (Kuttruff 1993) a perfectly reflective infinite cylinder with a source at its centre axis. Considering only the first reflection and discarding direct sound, he then calculates the root mean squared sound pressure in various receiver positions near the focusing area of the cylinder. In the present chapter we consider receivers in the same plane as the source (figure 14.1(a)). We first carry out simulations with the NURBS ray tracer using this cylinder as a case study. Figure 14.2 shows the mean squared sound pressure in a series of receivers close to the sound source as estimated by the raytracer for a NURBS cylinder as well as cylinder polygons of increasing number of faces using equations 14.3 and 14.4. The results are also compared with a geometrical approximation of the correct results near the source as described in (Kuttruff 1993). This approximation is defined by the following equation:

$$p_{rms}^2 = \frac{\rho c \cdot P}{4\pi \cdot a \cdot z} \tag{14.5}$$

where a is the cylinder radius and z is the receiver distance from the source.

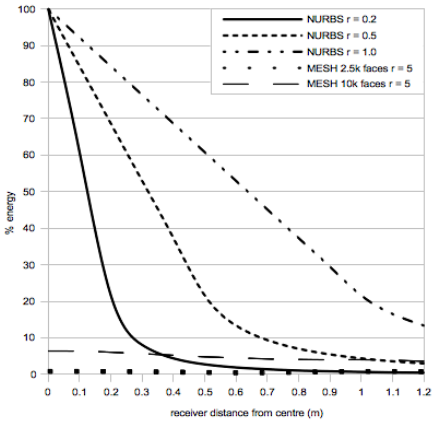

Figure 14.3: Sphere study - Percentile energy in relation to receiver distance from centre for NURBS and mesh geometry, with various receiver radii.

The geometrical approximation is not valid at the centre point (source position) because it results in infinite pressure. We can see that the NURBS results are close to the geometrical approximation, and we can also see that the number of faces necessary to approximate the NURBS result is over 1000 faces. This number is considerably lower if we use the Image Sources method (Kuttruff 1993). Like in any ray tracing simulation, the results are dependent on the receiver radius. A larger receiver volume will be able to detect a larger number of rays. Different acoustical simulators use different approaches from the one employed in this chapter, and their accuracy varies with changing rooms, receiver positions and ray paths (Xiangyang et al. 2003). This issue is not addressed in this PhD thesis, it is merely noted as part of the observations taken in the simulations.

14.3 Sphere Study

In (Vercammen 2010, 2012) Vercammen illustrates another case study of sound concentration from concave surfaces, this time involving a perfectly reflective sphere with a sound source at its centre (figure 14.1 (b)). Like in the cylinder example, only the first reflection is taken into account, attenuation, absorption from reflections and direct sound energy are neglected. In

this case we can expect 100% energy to return to the sphere centre, which provides us the opportunity to test the different geometrical models. Figure 14.3 shows the results of the NURBS and Mesh simulations with different receiver radius using:

$$P_{tot} = \sum_{i=1}^{N} P_{i,m} = \sum_{i=1}^{N} \frac{l_{i,m}}{D_m} \left(\frac{P}{N} \right) \qquad \text{(W)} \tag{14.6}$$

Where P_{tot} is the total energy detected by the receiver. The y axis in Figure 14.3 reports a the percentage of emitted energy P that is detected by the receiver P_{tot}. Results outside the sphere centre vary with receiver size as bigger receivers will detect more rays. However, if all reflections are calculated correctly, in the exact sphere centre all rays should go through the receiver perpendicularly and $l_{i,m}$ must be equal to D_m making $l_{i,m}/D_m = 1$. Thus with the correct ray reflection angles, the receiver size in the centre of the sphere is not relevant to the result. Figure 14.3 shows that at the sphere centre all NURBS calculations converge into 100% energy, proving a correct reflections in this geometrical model. Mesh calculations on the other hand, differ from receiver size and are far from 100% energy at the centre.

The root mean squared sound pressure in the focal point is explained in (Vercammen 2012) and calculated as follows:

$$p_{rms}^2 = \frac{1}{2} \hat{p} k^2 (1 - cos\theta_m)^2 \tag{14.7}$$

where $\hat{p}$ (N/m) is the amplitude descriptor that represents the pressure at 1 meter from the monopole source, k is the acoustic wave number and θ_m is the opening angle of the spheric segment, in the case of the full sphere $\theta_m = \pi$.

Formula 14.7 takes into account sound frequency by introducing the wave number k. Considering a frequency of 1000Hz, for a sphere and $\hat{p} = 1$(N/m) we get a ms pressure value of 73.27 (Pa^2), corresponding to an SPL of 112.6 (dB). Vercammen suggests a frequency dependent receiver diameter of $\lambda/2$. If we carry out this experiment in the center with a receiver of $\lambda/2 = 17$ cm an SPL of 120 dB is obtained. The receiver diameter to best approach the correct value has a diameter of 40 cm with an SPL of 112.7dB. As it is pointed out in (Vercammen 2012) this calibration of receiver size is impossible in cases where the exact value is unknown beforehand. However with a $\lambda/2$ receiver diameter a good approximation can be made.

Figure 14.4 shows the influence of receiver sizes in the sphere case study by plotting SPL in various receivers near the centre. NURBS geometry

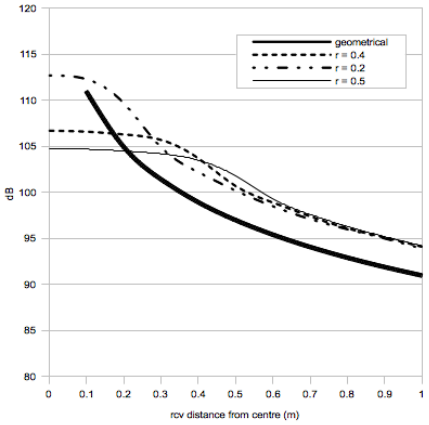

Figure 14.4: Sphere with a 10 m radius SPL (dB) in relation to receiver distance from centre with various receiver radius.

results are compared to a geometrical approximation described in (Vercammen 2012) and then converted to SPL. As in the cylinder example, this geometrical approximation is not valid in the centre, for the centre values we use:

$$p_{(z)^2 rms} = \frac{1}{2}\hat{p}/z^2 \qquad \text{(Pa)} \tag{14.8}$$

14.4 Ellipsoid Study

A similar series of simulations is done using an ellipsoid surface, the object in this case being to study the number of flat surfaces necessary to approximate the result obtained at the focusing area by the NURBS surface in a double curvature case. The sound source was placed in one of the ellipsoid's foci, and the receivers in the axis of the second focus (figure 14.1 (c)). Like in the case of the sphere, here too we can conclude that all rays should pass through a single point, in this case the focus opposite the source, therefore the receiver at this focus should detect 100% of the energy emitted by the source. Figure 14.5 shows that a mesh model with 10.000 faces has a result that is still far from correct, not reaching 20%. Mesh geometry with more

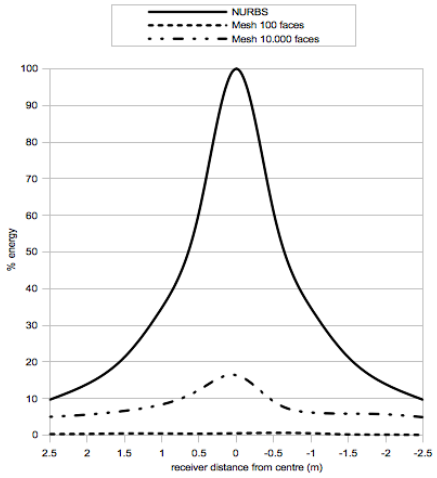

Figure 14.5: Ellipsoid study resutls Percentile energy in relation to receiver distance from ellipsoid focus, for NURBS and Mesh geometry with various number of mesh faces. All simulations done with a receiver of radius 0.5.

than 10.000 faces were not investigated for computational complexly reasons. NURBS geometry on the other hand shows a perfect 100% result when the receiver is placed in the second focus point.

14.5 Concave Surface Study Conclusions

The results of the concave examples show that NURBS representation of curved surfaces significantly improve the capability of acoustic simulation to predict sound concentration, because ray reflections are exact in curved surfaces without need for discretization.

The amount of planar sections required for accurate results in a ray-tracing model is not frequency dependent (Vercammen 2010), and it is also dramatically larger for double curvature surfaces when compared to single curvature.

Comparing results from the NURBS simulations to various mesh simulations, it's evident that increasing the number of segments improves the results, but in order to achieve reasonable results, the number of segments becomes unfeasibly large for current computational tools.

15

Early Sound Analysis of concert halls

When it comes to the design of concert halls and auditoria, the collaboration between architects and acoustic consultants can be difficult if one considers that they are both trying to define the form of the room but with completely different and sometimes contrasting priorities*.

As shown in previous chapters, computational acoustic simulation software is capable of estimating the impulse response and room acoustics parameters at receiver positions for diverse rooms with a good degree of accuracy. However these tools on their own do not give designers an idea as to the direction to take to improve results, nor do they help explore new room shapes.

Recent designs for concert halls around the world by renowned designers have prominently featured complex curved geometry. Concert hall designers have long employed convex surfaces in concert halls and concave surfaces in outdoor concert spaces, their potential to distribute energy where is needed has been proven by many examples (Vercammen 2012). Like any concave surface, complex double curvature surfaces need to be carefully studied and optimized to obtain desirable sound reflections and avoid sound concentrations.

In this chapter a form exploration tool is proposed, that can help designers and acoustic consultants interact with complex geometry and generate forms that can potentially distribute early sound energy in an optimal way.

*The contents of this chapter were published in the proceedings of the International Symposium on Room Acoustics 2013 in Toronto (Méndez Echenagucia, Astolfi, Shtrepi, van der Harten & Sassone 2013*b*)

15.1 Room Shape and Early Sound

Early reflections in concert spaces have been determined to be crucial to the overall acoustic quality by many researchers in the past (Barron 1971, Marshall 1994, Jurkiewicz et al. 2012, Patynen et al. 2013), and the characteristics of early sound are very dependent on the room shape, while the late sound energy is more dependent on average room absorption (Bradley 2011).

15.1.1 Insufficiency of Room Acoustics Parameters

ISO 3382-1 acoustic parameters are commonly used for the design of concert halls, but they are perhaps not detailed enough to describe the early portion of the sound that arrives at the listeners. Researchers have said that these indexes are insufficient to describe in detail the early sound, and that there are rooms with identical index values at various positions that have quite different subjective perceptions (Patynen et al. 2013, Bradley 2011, Bassuet 2011).

15.1.2 Studies and visualization methods of early sound

Research on the perception of early sound showed the importance of the first milliseconds in the overall perception of sound. Pioneering work by Haas determined echo audibility thresholds and the precedence effect (Haas 1951). He emphasized the importance of the first 30 milliseconds and the subjective perception of loudness. Barron later studied the effects of a single first reflection from side walls and ceilings (Barron 1971). He was able to study specific thresholds, source broadening and subjective impressions for side walls and ceilings. This study emphasized the importance of early lateral reflections.

Hidaka et al. published a comparison between shoebox and vineyard rooms that highlighted the importance of energy arriving in the first 80 milliseconds (Hidaka et al. 2008). They state that successful rooms show high sound strength in this first 80 milliseconds, corresponding a good amount of early reflections, and a high G_{early}, this is also mentioned by Bradley in (Bradley 2011). Hidaka et al. go on to say that before the first 80 milliseconds (for the 500 and 1000 Hz frequency bands) reflections angles and localization are perceived more accurately, reflections after 80 milliseconds are perceived by listeners as enveloping energy.

Different methods have been developed to study and visualize early sound. They show different levels of detail and have different specific purposes, but they all give us information about the early sound that we do not find in ISO 3382-1 acoustical indexes (Marshall 1994, Patynen et al. 2013, Bassuet 2011, Krokstad et al. 1968, Oguchi et al. 1988). Some of these studies have been done using measured impulse responses in existing concert halls to better understand their objective qualities while others are especially developed for design purposes and employ computational acoustic simulations. These methods help us understand differences in acoustical qualities, but they do not have ideal or optimal values for design purposes, as they have not all been compared to ideal existing conditions.

15.1.3 Uniform distribution of sound energy in time and space: A multi-objective problem

Acoustics parameters and measurements can be quite detailed when it comes to the distribution of energy in time. Early to late ratios (C_{50},C_{80}) for example are widely used and optimal values have been prescribed, but all of these indexes take single receiver positions into account. However, as previously stated and studied in the distribution chapters, the overall quality of a room cannot be summarized by index values in one single position, or a few advantaged positions close to the sound source. A good room considers the quality in all listening positions.

The distribution of sound energy in space and time poses a complex geometrical problem, reflections have to be directed in such a way as to provide sound energy uniformly over space and with time intervals in such a way as to satisfy subjective preferences. With a limited amount of energy being emitted by a given source, our goal is to generate room shapes that produce plenty of reflections in desirable time intervals over the whole listening area. We can say that room shapes that direct energy to the audience in the first milliseconds are in direct contrast to shapes that direct energy later in time. Hence, generating forms that evenly distribute energy in time and space is a multi-objective problem.

15.1.4 Time-Windows

In their pioneering paper in raytracing acoustical simulation, Krokstad et al. proposed the subdivision of sound reflections in rooms into "time-windows" that contain the reflections inside given time intervals (figure 15.1)(Krokstad et al. 1968). We can also consider receiver dependent time-windows in which

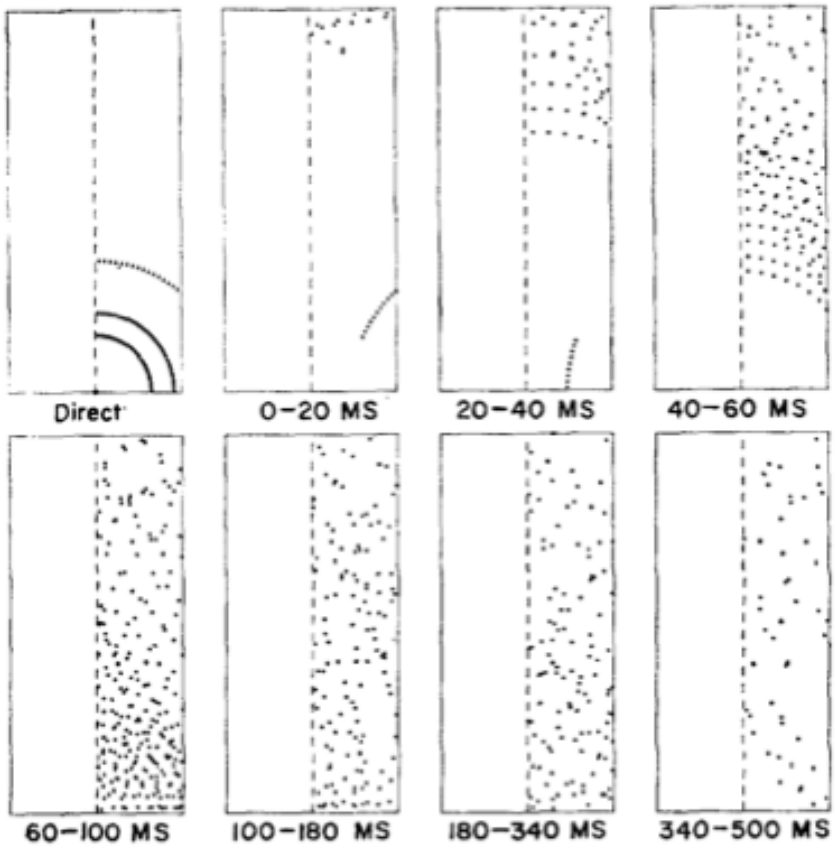

Figure 15.1: Krokstad's Time-Windows - An example of a spatio-temporal analysis.

time intervals are calculated from the arrival of the direct sound to each particular receiver. Time is counted by the algorithm from the arrival time of the direct sound of each receiver. By dividing the energy that arrives at the listening positions into time window we can study how rooms distribute energy in time, and evaluate the uniformity of this energy in the space of the audience area.

15.2 Tool for the uniform distribution of early sound in concert spaces

In this chapter a multi-objective genetic algorithm capable of finding room shapes that evenly distribute sound reflections in time and space using a NURBS based raytracing acoustic simulator is presented. This tool follows the same basic method described above in the structural case studies, with the exception that the fitness functions is calculated by a raytracing simulator and an acoustic study both developed for this PhD thesis by the author. A MOGA coupled with a parametric model and the acoustic simulator are employed to search for high-performing solutions.

15.2.1 The Ray tracing NURBS simulator

In the previous chapter a NURBS ray-tracing acoustic simulator was presented for the study of concave surfaces. The raytracer developed for this PhD thesis was also employed in the study of early reflections and complex curved geometry presented in this chapter. As was previously stated a class of python functions in combination with Rhinoceros comprises the raytracer. This class is able to cast rays into complex and free-form NURBS geometry and to plot their path, as well as create flat receivers that can detect ray reflections inside their area. The algorithm separates the reflected sound rays into time-windows that are calculated after the arrival time of the direct sound for each receiver. Since this study is about sound reflections, the direct sound rays are deliberately taken out of the simulation. Rays are reflected from the room surfaces until the travel time of the ray exceeds the time windows considered in the study, or until the ray reaches the audience. This means the rays are only allowed to reach the audience area once.

15.2.2 Acoustical fitness functions

MOGAs are capable of optimizing several objectives or fitness functions, through the combination of design variables. Fitness functions and design variables need to be well formulated by the designer in order for the MOGA to properly search for optimal solutions. In this chapter we are studying the distribution of sound energy in time and space, so we formulated 3 fitness functions based on the time-windows explained above.

The first fitness function considered a time-window from t_0 to t_1 in milliseconds (where instant t_0 is considered to be after the arrival of direct sound), the second from t_1 to t_2, and the third from t_2 to t_3.

The specific values for t_1, t_2 and t_3 should be chosen in the basis of the specific case being studied, for example, cases involving ceilings, side-walls, canopy reflectors or balconies can have different windows into account. The actual number of time-windows can also be specifically taylored for each design problem.

The uniform distribution of energy in space is the objective of each Fitness Function. For each time window the following equation was used to estimate the ideal amount of reflections for each receiver:

$$R_r = \frac{R_{tot}}{N_w \cdot N_r} \tag{15.1}$$

where R_r is the ideal number of reflections for each receiver inside a time-window, R_{tot} is the total number of rays emitted by the source, N_w is the number of time-windows and N_r is the number of receivers. With this ideal value of reflections in each receiver, we can calculate an error function that tells us how far is the room from an ideal reflection pattern for that time window:

$$E_{tot} = \sum_{i=1}^{N_r} |R_r - R_i| \tag{15.2}$$

where E_{tot} is the total error for the time-window and R_i is the number of rays in the i_{th} receiver. Equation 15.2 describes the fitness function that was used for each time window. The use of the absolute value of the difference $R_r - R_i$ means that the fitness function evaluates if the solution given errs by giving each receiver too many or too few ray reflections.

The minimization of these 3 fitness functions guarantees that the room shape found in the process delivers an equal amount of ray reflections in each time-window and also in each receiver. Thus ensures that the room

will provide sound reflections in all time windows, and that there will be no sound concentrations or shadowed areas anywhere in the audience area.

15.3 Case Study 7: Complex curved ceiling for a concert hall

The potential of the proposed design tool is explored by studying a shoebox concert hall with a curved reflective ceiling. The object of the study is to generate ceiling shapes that evenly distribute early sound energy oven the audience space and over 3 separate time-windows. The above mentioned ray-tracing algorithms for NURBS surfaces and the early sound analysis tools were employed, in combination with NSGA-II and a parametric model.

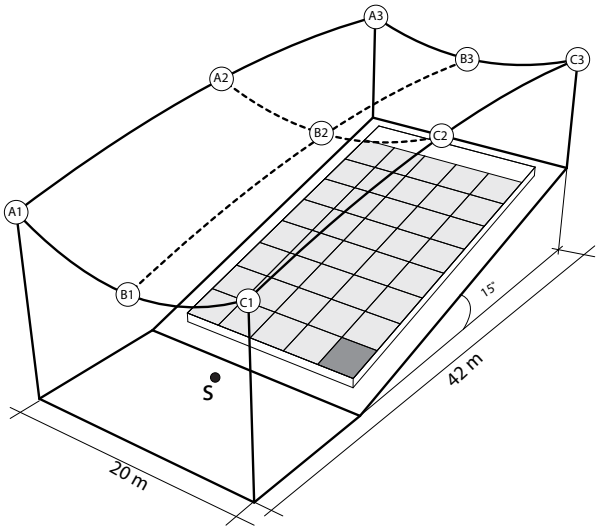

Figure 15.2: Parametric model for the acoustic ceiling case study.

15.3.1 Parametric Model

In any MOGA a set of design variables is needed to search for optimal solutions. In the case of acoustic geometry, design variables should define

Variable	Control Points	Movement Axis	Range of Movement
x_1	A1 and C1	Z	5 to 20m
x_2	B1	Z	5 to 20m
x_3	A2 and C2	Z	10 to 20m
x_4	B1	Z	10 to 20m
x_5	A3 and C3	Z	10 to 20m
x_6	B3	Z	10 to 20m

Table 15.1: Design variables, axis of movement and range of movement.

the changing geometry we want to evaluate, (for example we can use height, width and length dimensions for shoebox optimization). The case study presented in this chapter works with NURBS geometry to generate complex curve reflecting surfaces. These surfaces are specified by control points, and each control point is defined by its X, Y and Z coordinates. The case study described bellow employs fixed values of X and Y for all control points, and the Z values of these points are our design variables. Figure 15.2 shows the shoebox with a curved reflective ceiling defined by 9 control points. Design variables in geometric problems are always confined to a domain or range of movement, in order to limit the search possibilities, saving calculation times, and also to avoid undesired geometry.

Table 15.1 shows the design variables for the present study, their movement coordinates and range of movement. This parametrization of the shoebox ceiling ensures that the MOGA is capable of generating single and double curvature surfaces, both concave and convex towards the audience. Surfaces will always be symmetrical in the longitudinal axis of the room, and the area of ceiling above the stage can reach a height of just 5 meters if desired. If all design variables are equal, a flat ceiling is obtained, thus this study also considers the possibility that curved surfaces are not better than flat ones.

A single omnidirectional spherical source was employed. The audience has an inclination of 15 degrees from the stage plane. The audience area was subdivided into 40 flat segments of equal width and length.

15.3.2 Fitness functions

The total error function described in equation 15.2 was used as a fitness function for 3 different time-windows. The time-windows used in this case

study are described in the following table:

Time-window	t_{start} (ms)	t_{end} (ms)
1	0	80
2	80	120
3	120	200

Since there are 3 time-windows in this problem, there are 3 fitness functions. As we have seen above, NSGA-II can handle a high number of fitness functions and is capable of finding a Pareto set for the problem. The multi-objective problem studied in this case study can therefore be described with the following set of equations:

$$Case\ Study\ 7 \begin{cases} Minimize & f_{1(x)} = E_{tot,0-80}, \\ Minimize & f_{2(x)} = E_{tot,8-120}, \\ Minimize & f_{3(x)} = E_{tot,120-200}, \\ subject\ to & 5 \leq x_{1,2} \leq 20. \\ & 10 \leq x_{3-6} \leq 20. \end{cases} \tag{15.3}$$

15.3.3 Genetic algorithm inputs

NSGA-II explores 100 generations with 10 individuals in each generation. The overall genetic inputs for this case study is as follows:

Case Study 7		
Population Size (N)	10	
Number of Variables	6	
Number of binary digits	8	
Variable Domains	$x_{1,2} \in [5, 20]$	$x_{3-6} \in [10, 20]$
Mutation Probability (p_m)	0.2	
End Condition	End after 100 generations	

15.3.4 Results

Figures 15.3 and 15.4 show the ray distribution in the audience area for the 3 time windows of a series of room shapes, all belonging to the Pareto Front of solutions found by our design tool. We can see that the shapes obtained by the MOGA are varied and leave plenty of options for the architect and acoustical consultant to consider. Fitness values for each window are better in some individuals that in others, this is due to the fact that optimizing

rays for one window means there are fewer rays left over for the others, hence this is a true multi-objective problem with contrasting functions.

Solution 8 has the minimum value for window 1 and has good values for the other time windows, however it does neglect the first rows in the second window. Solution 5 has the minimum value for window 2, but it causes sound concentration in the first rows for window 3. Solution 3 has the minimum value for window 3 and has also good values for the other two windows. Solutions 0 and 2 are good intermediate solutions that have low E_{tot} values for all 3 windows.

15.3.5 Conclusions

An interactive acoustic search design tool is presented. It is capable of generating surface shapes that evenly distribute reflected rays in given time-windows and receiver areas.

Different shapes are better at distributing energy in particular time-windows than others, geometrical characteristics benefit certain areas of the room, and designers can consider the advantages of all suggested geometry.

Results show that the fitness functions formulated in the case study were in fact contrasting functions, hence a multi-objective approach is necessary to minimize all of them.

The effects of such distribution of sound energy towards the generally absorptive audience area has on later sound energy and reverberation needs to be further investigated.

Future research in this method should consider side-walls to study the 0-30 time-window (precedence effect, see (Haas 1951)).

More complex geometries and other concert hall typologies could be explored using the above described method, in order to study innovative room configurations. The possibility of incorporating the spatial aspects of early sound into this approach is also an interesting topic for further studies.

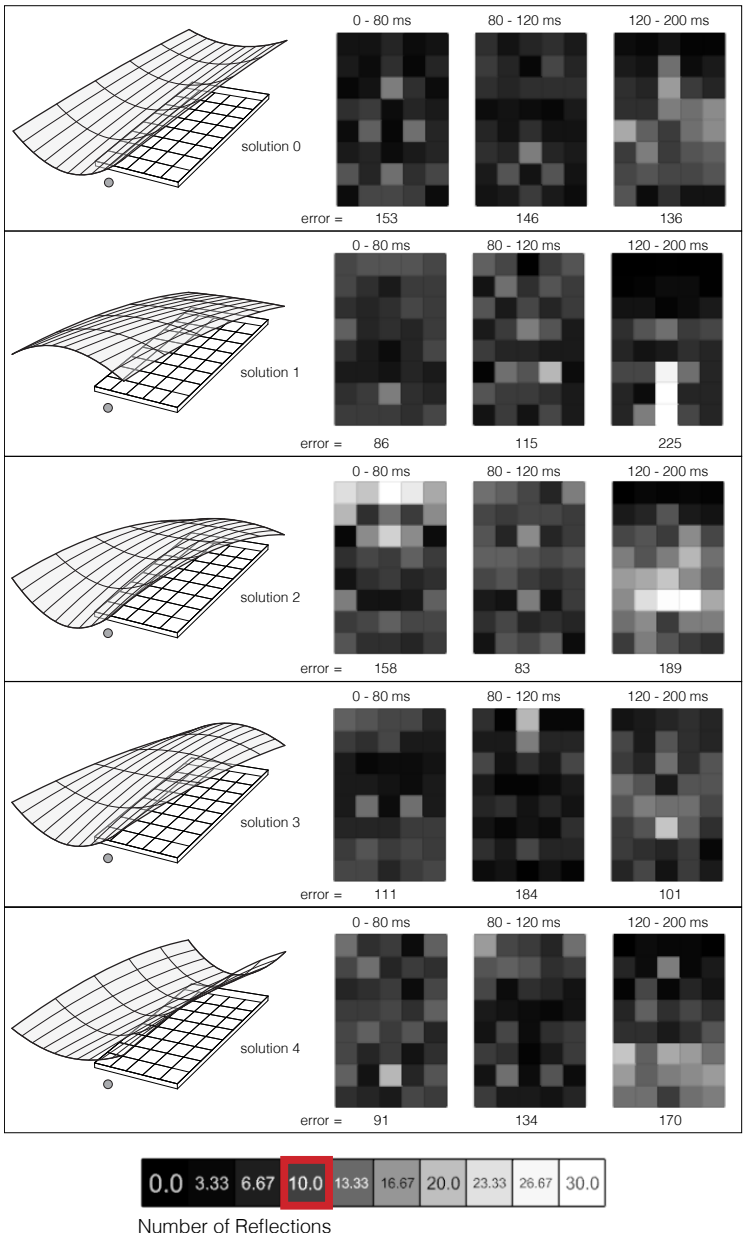

Figure 15.3: Distribution of reflected rays inside time-windows of a Pareto set of solutions for a Shoebox room with a reflective curved ceiling - Generated Curved Ceiling Shapes.

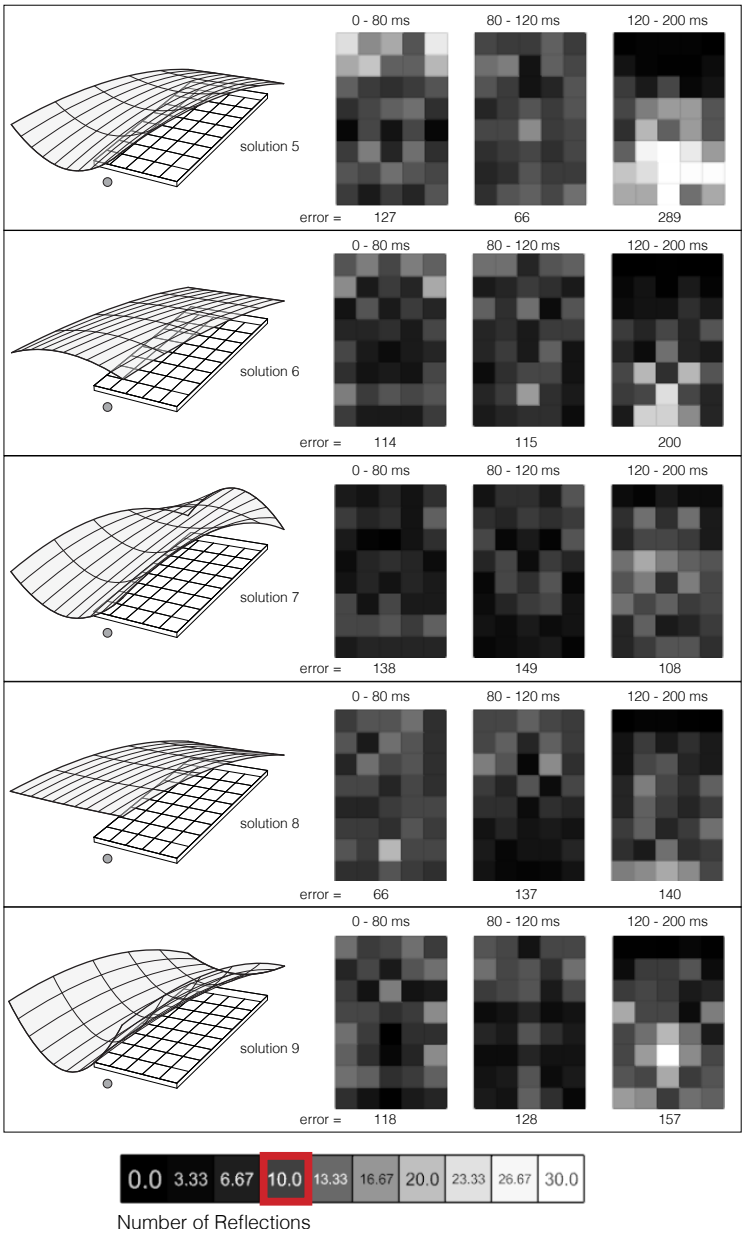

Figure 15.4: Distribution of reflected rays inside time-windows of a Pareto set of solutions for a Shoebox room with a reflective curved ceiling - Generated Curved Ceiling Shapes.